Saltational Episodes of Reticulate Evolution in the Drosophila saltans Species Group

Carolina Prediger, Erina A Ferreira, Samara Videira Zorzato, Aurélie Hua-Van, Lisa Klasson, Wolfgang J Miller, Amir Yassin, Lilian Madi-Ravazzi

Discoveries

Saltational episodes of reticulate evolution in the *Drosophila saltans* species group

Carolina Prediger[1,2], Erina A. Ferreira[2], Samara Videira Zorzato[1,3], Aurélie Hua-Van[2], Lisa Klasson[4], Wolfgang J. Miller[5], Amir Yassin[2,3*] and Lilian Madi-Ravazzi[1*]

[1]Department of Biology, UNESP - São Paulo State University, São José do Rio Preto, São Paulo, Brazil.

[2]Laboratoire Évolution, Génomes, Comportement et Écologie, CNRS, IRD, Université Paris-Saclay, Gif-sur-Yvette, France.

[3]Institut de Systématique, Évolution, Biodiversité (ISYEB), CNRS, MNHN, EPHE, Sorbonne Université, Univ. des Antilles, Paris, France.

[4]Molecular evolution, Department of Cell and Molecular Biology, Science for Life Laboratory, Uppsala University, Sweden.

[5]Center for Anatomy and Cell Biology, Department of Cell and Developmental Biology, Medical University of Vienna, Austria.

[*] These authors contributed equally.

Correspondence: amir.yassin@universite-paris-saclay.fr; lilian.madi@unesp.br.

Running title: Phylogenomics of the *Drosophila saltans* group

Conflict of interest

The authors declare no conflict of interest.

Data availability statement

Scripts used in this study, assemblies and intermediate files are publicly available on Figshare (https://doi.org/10.6084/m9.figshare.c.7100635.v1). Genome sequences generated for this study are available on NCBI BioProject: PRJNA1078835.

Acknowledgments

This paper is dedicated to Prof. Hermione E. M. C. Bicudo for her significant contributions to the study of the evolutionary genetics of species of the *Drosophila saltans* species group. We would like to thank David Ogereau for his assistance and insights in genome assembly for this study. We thank Fundação de Amparo à Pesquisa do Estado de São Paulo (FAPESP) for the financial support to L.M.R. (Number processes: 95/06165-1, 2014/14059-0 and 2016/ 11994-5) enabling us to collect and sequence many strains used here. We extend our thanks to the Conselho Nacional de Desenvolvimento Científico e Tecnológico (CNPq) for their support, specifically grant number 141545/2020-8, as well as the France Excellence Eiffel Scholarship Program for funding C.P.'s PhD scholarship. *Illumina* sequencing of *D. neocordata* was performed at the SNP&SEQ Technology Platform in Uppsala, Sweden, which is part of the Swedish National Genomics Infrastructure and Science for Life Laboratory. SNP&SEQ is supported by the Swedish Research Council and the Knut and Alice Wallenberg Foundation. This project was partly supported by a grant from The Swedish research council VR (2014-4353) to L.K. We want to thank the Nouragues research field station (managed by CNRS), which benefits from “Investissement d'Avenir” grants managed by Agence Nationale de la Recherche (AnaEE France ANR-11-INBS-0001; Labex CEBA ANR-10-LABX-25-01). The project was partly funded by the Austrian Science Fund FWF grant P28255-B22 to W.J.M. and by the Richard Lounsbery Foundation, ANR-18-CE02-0008, and ANR-19-CE34-0011 to A.Y.

Abstract

Phylogenomics reveals reticulate evolution to be widespread across taxa, but whether reticulation is due to low statistical power or it is a true evolutionary pattern remains a field of study. Here, we investigate the phylogeny and quantify reticulation in the *Drosophila saltans* species group, a Neotropical clade of the subgenus *Sophophora* comprising 23 species whose relationships have long been problematic. Phylogenetic analyses revealed conflicting topologies between the X chromosome, autosomes and the mitochondria. We extended the ABBA-BABA test of asymmetry in phylogenetic discordance to cases where no "true" species tree could be inferred, and applied our new test (called 2A2B) to whole genome data and to individual loci. We used four strategies, two based on our new assemblies using either conserved genes or ≥50 kb-long syntenic blocks with conserved collinearity across Neotropical *Sophophora*, and two consisted of windows from pseudo-reference genomes aligned to either an ingroup or outgroup species. Evidence for reticulation varied among the strategies, being lowest in the synteny-based approach, where it did not exceed ~7% of the blocks in the most conflicting species quartets. High incidences of reticulation were restricted to three nodes on the tree, that coincided with major paleogeographical events in South America. Our results identify possible technical biases in quantifying reticulate evolution and indicate that episodic rapid radiations have played a major role in the evolution of a largely understudied Neotropical clade.

Keywords: phylogenomic discordance; genome assembly; historical biogeography; introgression; cyto-nuclear conflicts; Neotropical speciation; *Sophophora*.

Introduction

Knowledge of phylogenetic relationships among species is a requirement for many evolutionary studies. However, it is often difficult to reconstruct well-resolved bifurcating trees for some clades. This could either be due to the lack of signal in the evaluated data, a condition known as "soft polytomy", or due to persistent phylogenetic conflicts among datasets leading to "hard polytomies" and reticulate patterns of interspecific relationships. A plethora of biological processes could cause such conflicts, including incomplete lineage sorting (Maddison 1989; Maddison 1997; Walsh et al. 1999; Townsend et al. 2012), horizontal gene transfer, introgression and hybridization (Schrempf and Szöllősi 2020), and adaptive radiations (Glor 2010). Phylogenetic conflict may also be caused by technical errors, such as, sequencing error, contamination, wrong model selection and general lack of quality control (Philippe et al. 2011). Recent advances in genomic analyses have significantly reduced such errors and, in a wide range of taxa, increased the number of analyzed genes hence helping to resolve early conflicting topologies. However, in many other cases, whole genome analyses demonstrated persistent phylogenetic conflicts (e.g., in plants (Wickett et al. 2014; Gagnon et al. 2022), birds (Suh 2016), sponges and ctenophores (Philippe et al. 2009; Pick et al. 2010; Chang et al. 2015; Whelan et al. 2015; Simion et al. 2017), mammals (Morgan et al. 2013; Romiguier et al. 2013; Doronina et al. 2015), amphibians (Hime et al. 2021), and insects (Owen and Miller 2022)).

Of the different processes that can reduce phylogenetic resolution, introgression has attracted much attention, and led to the development of a number of bioinformatic tools and tests that quantify its extent across the genome (Durand et al. 2011; Pease and Hahn 2015; Malinsky et al. 2021). Site-based methods usually count the number of bi-allelic sites supporting each of three possible topologies in a species triplet with an outgroup (Figure 1A). Comparisons between the proportions of the three topologies can yield one of four possible

94 outcomes (Figure 1B): (i) complete trifurcation, all topologies are equally encountered; (ii)
95 incomplete trifurcation, such as in the case of hybrid speciation wherein two topologies
96 significantly exceed the third one but do not significantly differ from each other; (iii)
97 incomplete bifurcation, such as in the case of asymmetric introgression wherein the
98 proportion of all topologies significantly differ; and (iv) complete bifurcation, one topology
99 significantly exceeds the two others, which in their turn have nearly equal proportions.
100 Categories ii and iii are often considered to evidence reticulate evolution. The earliest of
101 introgression tests, ABBA-BABA or the Patterson's *D* statistic (Green et al. 2010; Durand et
102 al. 2011), compared the two later cases (iii and iv), *i.e.* it presumed that a "true" species tree
103 exists. A later test, HyDe (Blischak et al. 2018), quantifies admixture (γ) from the ratio of
104 shared alleles with the test going from 0 (full isolation) to 0.5 (full hybridization) and
105 therefore it can also cover case ii. The two tests differ in how they measure significance, using
106 jackknifing or bootstrapping in Patterson's *D* and normal approximation in HyDe. Of late,
107 another site-based test was developed using χ^2 to test for deviation of parity between the three
108 topologies as in case i (Sayyari and Mirarab 2018). A unified test that can test the prevalence
109 of each of the four categories across the genome is still lacking.
110 Reminiscent to the problem of soft and hard polytomies, wherein the statistical power
111 of a phylogenetic analysis largely depends on the size of a locus, interpreting reticulation is
112 largely influenced by how a locus is defined. For example, at the species level, an analysis on
113 a whole concatenated alignment of a quartet should have a greater power (*i.e.* a total evidence
114 approach). However, sites are often physically linked and evolutionarily-dependent.
115 Consequently, whole genome analyses may be biased towards genomic regions with more
116 variable sites (Martin et al. 2015). Therefore, phylogenetic analyses are usually conducted at
117 individual loci under the multispecies coalescent model, which often outperforms
118 concatenation in multiple groups of animals (Jiang et al. 2020). In theory, a window size of

~100-kb long is appropriate to overcome the non-independence of sites under realistic recombination rates (Pease and Hahn 2015), but the definition of such windows would largely depend on the taxonomic scale of the analysis. For example, at shallow phylogenetic depths, it is customary to use a pseudo-reference genome approach, whereas reads from multiple species are aligned to a reference genome (Sarver et al. 2017). Here, the distance from the reference genome species can greatly influence the quality of mapping and subsequent analyses due to potential gene duplications and rearrangements (Rick et al. 2023). Alternatively, single-copy orthologous genes, such as those that have been popularized by the BUSCO program (Manni et al. 2021), can be used (Suvorov, Kim, et al. 2022; Suvorov, Scornavacca, et al. 2022). However, such gene are presumably under strong selection, with the relaxation of selection in some lineages may conflate introgression estimates (Frankel and Ané 2023). Longer syntenic blocks may be a better choice to maintain the advantages for methods based on conserved orthologous genes while adding information from less conserved, longer non-coding regions in these blocks. However, the use of such blocks in introgression analyses has not, to the best of our knowledge, been explicitly investigated.

Phylogenetic conflicts have been reported for the jumping fly *Drosophila saltans* species group, a clade of the subgenus *Sophophora* with 23 Neotropical species (Magalhães 1962; Bächli 2024). The group retains its name from the peculiar "jumping" habit of its larvae; *"the larva seizes its posterior end with its mouthhooks, and stretches. The hooks pull loose suddenly, the larva straightens with considerable force, and as a result is thrown several inches into the air"* (Sturtevant 1942). The group was divided into five species subgroups, namely, *saltans, parasaltans, cordata, elliptica* and *sturtevanti* subgroups, mostly on the basis of male genitalia (Magalhães and Björnberg 1957). Although the monophyly of the subgroups has been confirmed by different phylogenetic methods, the relationships among and within them are not. Hypotheses for their evolutionary relationships have been proposed

using different methods and different morphological characters (Magalhães and Björnberg 1957; Throckmorton 1962; Throckmorton and Magalhães 1962; O'Grady et al. 1998; Yassin 2009; Souza et al. 2014; Roman et al. 2022), chromosome polymorphism (Bicudo 1973a), reproductive isolation (Bicudo 1973b; Bicudo and Prioli 1978; Bicudo 1979), protein polymorphism (Nascimento and Bicudo 2002) and gene sequences (Pélandakis and Solignac 1993; O'Grady et al. 1998; Rodríguez-Trelles et al. 1999; Castro and Carareto 2004; de Setta et al. 2007; Roman et al. 2022). The evolutionary relationships proposed are summarized in Supplementary Table S1.

Unlike other species groups in the subgenus *Sophophora*, such as the *melanogaster*, *obscura* and *willistoni* groups, genomic resources and genetic investigations in the *saltans* species group are scarce. Indeed, only four genomes have been sequenced and assembled to date (Kim et al. 2021). To bridge this gap and to test for the extent of phylogenetic conflicts, we sequenced and assembled genomes for 15 species with representatives from the five subgroups. Phylogenetic analyses using well-conserved genes resolved the evolutionary relationships among the subgroups but also highlighted conflicts between X-linked, autosomal and mitochondrial loci. To test how each of the four incongruence categories prevails across the species, we devised a new χ^2-based test that we called 2A2B. The test uses pairwise comparisons of the three topologies proportions shown in Figure 1. We applied this test to sets of conserved orthologous genes and to long syntenic blocks with conserved collinearity across the Neotropical *Sophophora*, as well as to 100-kb long windows from pseudo-reference genomes aligned to either an ingroup (*D. sturtevanti*) or outgroup (*D. willistoni*) species. We found reticulation levels to differ among the datasets and the subgroups, and to coincide with major historical biogeographical events in the Neotropics.

Results

Short-read assembly of 17 genomes recovered 90% of BUSCO genes

We sequenced using short-read Illumina approach 17 whole genomes from 15 species collected across various locations in the Neotropical region. Genome size, estimated from 21-kmer frequency spectrum using GenomeScope 2 (Ranallo-Benavidez et al. 2020), ranged from 154.0 to 356.8 Mb. Our de novo assemblies using MaSuRCA (Zimin et al. 2013) resulted in genome lengths ranging from 177.5 to 287.7 Mb, with N50 values ranging from 2 to 92 Kb (Supplementary Table S2). To evaluate the completeness of our assembled genomes, we searched for single-copy genes (SCG) using BUSCO (Simão et al. 2015). We found that over 90% of the searched genes were complete for all of the genomes (Supplementary Table S2). Kim et al. (2021) assembled using both short Illumina and long Nanopore reads the genomes of four *saltans* group species, all of which we have independently sequenced. Whereas their assemblies' contigs were much longer, with N50 ranging from 2 to 6 Mb, the BUSCO score for the same set of species did not largely differ (98% vs. 95-96% in our study; Supplementary Table S2). However, Kim et al. (2021) aimed at generating high quality reference which is not the purpose of this study.

Muller elements analysis resolves relationships between the subgroups and unravels a minor X-autosomal conflict in the sturtevanti subgroup

Phylogenomic analyses were performed using 2,159 SCG shared across all species. Gene trees, inferred for each SCG using maximum-likelihood in IQ-TREE (Minh et al. 2020) produced 1,263 distinct topologies, with 206 of them found more than once. To test if SCG chromosomal position may underlie the discrepancies in gene trees, we localized each SCG to its corresponding Muller element according to the position of its *D. melanogaster* ortholog identified by Blast (Camacho et al. 2009). As a result, we generated five independent datasets,

each corresponding to the Muller elements A, B, C, D, and E, comprising 337, 370, 425, 419, and 568 SCGs, respectively. These datasets were then used to reconstruct the species trees using the multi-species coalescent model, and the genes within them were concatenated for Bayesian and Maximum Likelihood phylogenetic inferences.

The trees generated by the 5 data sets showed very similar topologies with well supported nodes either in the Bayesian Inference implemented in BEAST (Bouckaert et al. 2019), the maximum-likelihood implemented in IQ-TREE, or for the multi-species coalescent model analysis implemented in ASTRAL-III (Zhang et al. 2018) (Supplementary Figures S1, S2 and S3). The *parasaltans* subgroup was placed as sister to all other subgroups, followed by the emergence of the *sturtevanti* subgroup. The *cordata* and *elliptica* subgroups showed a close relationship, and were sister to the *saltans* subgroup. The only discrepancy between the topologies was the placement of *D. lehrmanae*, a newly discovered species in the *sturtevanti* subgroup (Madi-Ravazzi et al. 2021). For this species, while maximum-likelihood and multi-species coalescent analyses reported lack of branch support for multiple trees (Supplementary Figures S2 and S3), Bayesian inference recovered well supported branches and two topologies (Figure 2A and Supplementary Figure S1). The two distinct topologies distinguished the Muller elements forming the X chromosome (elements A and D who are fused in a fusion shared by the Neotropical *Sophophora*, *i.e.* the *saltans* and *willistoni* groups (Sturtevant and Novitski 1941; Dobzhansky and Pavan 1943; Cavalcanti 1948), and the Muller elements representing autosomal chromosomes (elements B, C and E).

The published genome of *D. prosaltans* (Kim et al. 2021) did not group with the genome of this species sequenced by us, instead it grouped with *D. saltans*. The genome previously published comes from a line collected in El Salvador in 1957. According to Magalhães' (1962) detailed morphological revision of multiple geographical specimens of the *saltans* group, the sampling site of this particular strain is outside the geographical range of *D.*

prosaltans, but within the expected range of *D. saltans*. Furthermore, the *D. saltans* and *D. prosaltans* lines used in our study underwent thorough morphological analyzes (Souza et al. 2014; Roman and Madi-Ravazzi 2021), indicating that the lines we used were accurately identified. Therefore, it is likely that the previously sequenced *D. prosaltans* strain from El Salvador was misidentified and we consider it here to belong to *D. saltans*.

Mitogenomes show cytonuclear conflicts in the sturtevanti *and* saltans *subgroups*

We assembled mitochondrial genomes for the 15 *saltans* group species using MitoZ (Meng et al. 2019). We did not use the previously assembled four strains since several mitochondrial scaffolds were likely removed in those assemblies (Kim et al. 2021). We conducted phylogenetic analysis on the aligned mitogenomes genes using both IQ-TREE and BEAST. Overall, the mitochondrial trees matched the topology of the nuclear gene trees regarding the inter-subgroup relationships. However, three major discrepancies were identified (Figure 2B). First, the position of *D. lehrmanae* within the *sturtevanti* subgroup did not agree with either the X or autosomal SCG topologies, proposing a topology wherein *D. lehrmanae* is a sister species of *D. sturtevanti* (a topology recovered once in multi-species coalescent analysis (Muller element C, Supplementary Figure S3) and maximum likelihood (Muller element B, Supplementary Figure S2)). Second, whereas the mitochondrial tree recovered the monophyletic relationship between the *elliptica*, *cordata* and *saltans* subgroups, the position of *D. neocordata* (*cordata* subgroup) differed, being sister to the three species of the *elliptica* subgroup in the nuclear trees and to the six species of the *saltans* subgroup in the mitochondrial tree. Third, whereas nuclear trees recovered three lineages within the *saltans* subgroup, namely*, austrosaltans*, *nigrosaltans-pseudosaltans*, and *septentriosaltans-prosaltans-saltans*, only two lineages are revealed by the mitochondrial tree. Each of the mitochondrial clades involved one species from otherwise sister species in the nuclear trees,

i.e. D. nigrosaltans and *D. saltans* in one clade and their respective closely-related species *D. pseudosaltans* and *D. prosaltans* in the other clade, suggesting that multiple cytoplasmic introgression events might have occurred in this subgroup (Figure 2B). Because *D. saltans* and *D. prosaltans* are reported as sister species in the nuclear trees and are separated in the two mitochondrial clades, the two mitoclades were called *S* and *P*, respectively. Remarkably, the branching order in the *P* mitoclade is congruent with the nuclear tree, unlike the order in the *S* mitoclade. The *S* mitoclade may therefore be of reticulate origin, probably reflecting an older introgression from *D. austrosaltans* to *D. nigrosaltans* and a more recent introgression between *D. austrosaltans* and *D. saltans*. However, due to the particularities of mtDNA compared to nuclear genomes (see Discussion below), the incomplete lineage sorting of two major haplotypes in the ancestor of the *saltans* subgroup may have resulted in the evolution of the two mitoclades.

The extent of reticulation differs between assembly- and pseudo-reference-based approaches

To quantify the extent of introgression at a genome-wide scale, we analyzed allele distribution of bi-allelic phylogenetically informative sites in 28 species quartets using Patterson's *D* estimate of the standard ABBA-BABA test. We used four distinct locus-defining strategies to explore how strategy choice can influence estimates of *D*. Two strategies relied on our *de novo* genome assemblies. The first strategy included the use of single-copy genes (SCG) defined by BUSCO (2,159 loci). The second strategy identified syntenic blocks equal to or greater than 50 kb-long with collinearity across the 15 *saltans* assemblies and *D. willistoni*, *i.e.* across Neotropical *Sophophora* (1,797 loci). The third and fourth strategies used a pseudo-reference approach, wherein the reads of each *saltans* group species were mapped to an ingroup (*D. sturtevanti*, 2,328 loci) or an outgroup species (*D. willistoni*, 1,863 loci) and a pseudo-reference was inferred by replacing variant sites in the

reference genome by the ones in the reads (as in Mai et al. 2020). In these pseudo-reference strategies, a locus was defined as a 100 kb-long window of the reference genome. To avoid the influence of linked loci from highly-variable regions on genome-wide estimates, we randomly sampled 20 sites from each locus with ≥20 evaluated sites, and repeated resampling for 100 reiterations for each locus-defining strategy.

For a bi-allelic site, the standard ABBA-BABA (Patterson's *D*) test considers that a true species tree exists, with site distribution BBAA, and then evaluate the deviation from parity of the two discordant configurations ABBA and BABA. We found that genome-wide absolute Patterson's *D* estimates, *i.e.* $(\sum ABBA - \sum BABA)/(\sum ABBA + \sum BABA)$, greatly differed among the four strategies (Figure 3A). Synteny-based strategy had the lowest $|D|$ across the 28 quartets ($|D| = 0.025 \pm 0.004$) compared to BUSCO ($|D| = 0.066 \pm 0.014$, Student's t $P < 0.01$), *D. sturtevanti* pseudo-reference ($|D| = 0.176 \pm 0.025$, Student's t $P < 4.77 \times 10^{-6}$), and *D. willistoni* pseudo-reference ($|D| = 0.329 \pm 0.053$, Student's t $P < 5.97 \times 10^{-6}$). So, of the four strategies, the use of syntenic blocks is the most conservative.

To gain further insights on the reasons of this discrepancy between the four locus-defining strategies, we separately investigated assembly- and pseudo-reference-based approaches. The BUSCO approach mainly differs from the synteny-based approach in having, on average, shorter sequence since many loci are ≤50-kb long. Short sequences usually show faster lineage-specific evolutionary rates (Lipman et al. 2002), which can increase variance and also induce biases on Patterson's *D* due to the violation of the molecular clock assumption (Frankel and Ané 2023). Besides, the BUSCO analysis involves an additional step, which is the annotation of the conserved protein-coding genes (Manni et al. 2021). To account for these possible sources of errors, we counted for each lineage the number of singletons distinguishing the outgroup from the three ingroup species (*i.e.* BBBA sites), as well as the singletons distinguishing between the two most closely-related species in the

quartet as defined from the phylogenetic analyses above (*i.e.* BAAA and ABAA). we called this test 3A1B, and it is reminiscent to the classical Tajima's (1993) Relative Rate Test. Under the assumption of a constant molecular clock or the absence of mis-annotation of a BUSCO gene in one of the two sister species both BBBA – BAAA and BBBA – ABAA should be > 0. We focused on the *elliptica* subgroup with *D. saltans* as an outgroup (*i.e.* (((*emarginata*,*neoelliptica*),*neosaltans*),*saltans*)) quartet, since this quartet showed a strong discrepancy between the two assembly-based approaches, with genome-wide *D* being 0.25 for BUSCO and -0.08 for synteny-based strategy. By applying the 3A1B test, we found that 37 BUSCO loci violated its assumption, all in the negative direction for *D. emarginata*, *i.e.* BAAA > BBBA. By excluding these loci, Patterson's *D* dropped from 0.25 to 0.04. By contrast, only 5 loci violated the assumption in the synteny-based strategy. Their exclusion did not change Patterson's *D* estimate which remained -0.08. We then applied the 3A1B test for all locus-defining approaches, excluding loci that violated its basic assumption in each quartet. The genome-wide absolute Patterson's *D* estimates dropped from 0.066 ± 0.014 to 0.030 ± 0.004 for BUSCO genes (Student's *t* $P < 0.05$) and from 0.025 ± 0.004 to only 0.023 ± 0.004 for synteny-based loci (Student's *t* $P = 0.76$). After correction, genome-wide estimates from both BUSCO and synteny loci did not significantly differ (Student's *t* $P = 0.28$), even if synteny estimates remained slightly lower (Figure 3B).

For pseudo-reference approaches, excluding rapidly evolving loci through the 3A1B test may not be enough, since quality and depth of mapping as well as reference genome biases constitute additional sources of errors. We therefore reconducted the analyses using more stringent parameters, only retaining loci with a mapping quality >20 and a depth >10 and <100 and excluding all within-species polymorphic sites. These parameters dramatically reduced the number of evaluated loci to only 17% and 4% in the ingroup (*D. sturtevanti*) and outgroup (*D. willistoni*) reference genome approaches. Estimation of genome-wide absolute

Patterson's *D* dropped to 0.101 ± 0.023 (Student's *t* $P < 0.05$) and 0.102 ± 0.017 (Student's *t* $P < 2.9 \times 10^{-4}$) for the ingroup and outgroup references, respectively. This means that whereas ingroup and outgroup approaches were greatly different before the application of the stringent criteria (Student's *t* $P < 0.05$), absolute Patterson's *D* did not significantly differ between the two approaches after corrections (Student's *t* $P = 0.95$). For the abovementioned *elliptica* subgroup example, whereas before the stringent criteria Patterson's *D* were 0.02 and -0.71 for ingroup and outgroup approaches, these values dropped to -0.005 and -0.27 in the two approaches, respectively. However, correlation across quartets was strong (Pearson's $r = 0.56$, $P = 0.002$), indicating that distinct criteria may be applied to improve estimates depending on the distance from the reference genome species, with *D. willistoni* being more distant and hence prone to more variance due to the lower number of conserved loci that can be retained.

The 2A2B test unravels lower signal for introgression when syntenic blocks are used

To consider cases where a true species tree cannot be inferred, we designed a test that we call 2A2B. The test is an extension of the standard ABBA-BABA test in that it does not only test the significance of deviation from parity of the ABBA and BABA patterns, but also test the deviation from parity of each configuration to the BBAA pattern. Therefore, the test allows classifying each species triplet with an outgroup into one of the four categories along the trifurcation-bifurcation continuum given in Figure 1. We applied the test at both the genome-wide level after corrections using the 3A1B test and mapping criteria (see above).

We found that for all locus-defining strategies, bifurcation categories (iii and iv) predominated (Figure 4A). Only five exceptions were observed. One incidence of category ii (incomplete trifurcation) was observed in the BUSCO strategy concerning the position of *D. lhermanae* relative to both *D. sturtevanti* and *D. dacunhai*. Indeed, the position of *D. lhermanae* was the only conflicting result in the phylogenetic analyses based on BUSCO

genes and it also showed a conflict with mitochondrial analysis (Figure 2). Four incidences of category i (complete trifurcation) were observed in outgroup pseudo-reference strategy. Of which, two concerned the position of *D. lehrmanae* to both *D. sturtevanti* on the one hand and to each of the two sister species *D. dacunhai* and *D. milleri* on the other hand. The other two complete trifurcation cases concerned the relationships between the three lineages of the *saltans* subgroups, *i.e. austrosaltans*, *nigrosaltans-pseudosaltans*, *septentriosaltans-prosaltans-saltans*, in cases where species of the different mitoclades were analyzed together, *i.e. D. pseudosaltans* and *D. saltans* or *D. nigrosaltans* and *D. septentriosaltans* (Figure 2).

Category iv (complete bifurcation), which is the most consistent with a true species tree, was the most frequent in synteny-based strategy (Figure 4). This was followed by both the BUSCO and the outgroup pseudo-reference strategies but the difference in category iv frequency was not significant (Fisher's exact test of category iv vs. all other categories). However, with only four exceptions, ingroup pseudo-reference approach identified category iii (incomplete bifurcation), which mostly indicates cases of introgression, in all analyzed quartets (Fisher's exact test between synteny-based and ingroup pseudo-reference strategy $P < 1 \times 10^{-4}$). The total number of bi-allelic sites (20 per locus) that were used in the genome-wide analysis differed among the four strategies, averaging 22,893 (BUSCO) and 21,306 (synteny) in assembly-based approaches, and 35,747 and 5,308 sites for the ingroup *D. sturtevanti* and the outgroup *D. willistoni* pseudo-reference approaches, respectively. The low number for the *D. willistoni* pseudo-reference is expected since increasing mapping quality criteria on the genome of this distant species would only favor strongly conserved loci. For the *D. sturtevanti* pseudo-reference, applying the same mapping quality criteria has likely maintained less conserved loci. Although we have excluded heterozygous sites from every species to reduce mapping biases of the reference allele, such biases may even extend to homozygous sites strongly linked to the excluded heterozygous site in the same read.

Universal mapping criteria that can reduce mapping biases independent from the reference genome do not exist and mapping biases remain difficult to detect (Lin et al. 2024). However, these biases are the most likely explanation of the extensive signal of introgression in the ingroup *D. sturtevanti* pseudo-reference. To test the effect of mapping quality on introgression estimates, we applied the 2A2B test at the locus level before and after applying mapping quality thresholds. In agreement with our assumptions and the findings on Patterson's *D* (Figure 3), the proportion of loci supporting categories ii and iii, *i.e.* categories that are the most associated with reticulate evolution, did not exceed ~7% in assembly-based strategies, but they dropped after application of mapping quality criteria from 46% to 11% and from 34% to 4% for *D. sturtevanti* and *D. willistoni* pseudo-reference genomes strategies, respectively (Supplementary Figure S4). Ingroup pseudo-reference approaches, while providing more data, may not reflect the true phylogenetic relationships between the species, hence inflating the estimation of the extent of introgression.

Historical biogeographical events coincided with episodes of low phylogenetic resolution

Phylogenetic analyses and assembly-based 2A2B test identified three parts on the species tree with evidence for incomplete bifurcation (*i.e.* category iii): at the inter-subgroup level in any combination that involved representatives from at least two subgroups of the *cordata*, *elliptica* and *saltans* subgroups, at the base of the *sturtevanti* subgroup, and in the *saltans* subgroup in quartets involving species belonging to distinct mitoclades. Whereas category iii is usually interpreted as evidence of introgression following secondary contact, other biological processes such as ancestral population structure at the time of phyletic radiation or asymmetry of evolutionary rates due to responses to distinct adaptive pressures (Hibbins and Hahn 2022; Frankel and Ané 2023) can generate similar signals. Because all these processes can associate with major geographical changes affecting species distribution,

ecology and frequency of secondary contacts, a knowledge of the historical biogeography of the clade under study is crucial for the understanding of the processes that have likely led to phylogenetic conflicts.

Like phenotypic traits, ancestral geographical distribution can be inferred on phylogenetic trees from present day geographical data (Quintero et al. 2015). Therefore, we mapped current distribution of the studied species on the Bayesian X tree that was dated in reference to recent family-wide estimates (Suvorov, Kim, et al. 2022) (see Methods). The historical biogeography supported an origin of the *saltans* group around 16 million years (myr) ago in the north-west of South America, which currently corresponds to the Amazonian region (Figure 5). At that time, this region was dominated by a vast wetland environment known as the 'Pebas System.' The first radiation episode, *i.e.* the split between the ancestors of the *cordata*, *elliptica* and *saltans* subgroups occurred circa 10 myr ago at this region, coinciding with the formation of the Amazon River and its huge fluvial networks that led to the transformation of the Pebas wetland into the dense and diverse Amazonian forests (Hoorn et al. 2022). The second episode occurred nearly 3 myr ago, which correlates with the geological formation of the isthmus of Panama (O'Dea et al. 2016), and the time of a connection between the Western Amazonian and the Southern Atlantic rainforests during the Pliocene (Batalha-Filho et al. 2013; Ledo and Colli 2017). This episode involved the ancestors of the *nigrosaltans-pseudosaltans* and *septentriosaltans-prosaltans-saltans* clades. Indeed, the first clade has a northern to central representative (*D. nigrosaltans*) and a southern species (*D. pseudosaltans*), whereas the second clade has a northern representative (*D. saltans*) and two central and central to southern species (*D. septentriosaltans* and *D. prosaltans*, respectively). The third radiation episode involves the ancestor of the *sturtevanti* subgroup and also occurred in the late Pliocene, ca. 2.5 myr ago, at the likely time of a connection between the Western Amazonian and the Southern Atlantic rainforests.

Discussion

Towards a comprehensive phylogeny of the saltans species group

A large number of *Drosophila* genomes have been sequenced and used in phylogenetic analyses (Khallaf et al. 2021; Kim et al. 2021; Li et al. 2022; Suvorov, Kim, et al. 2022), but studies with comprehensive sampling of nearly all species in a group remain relatively uncommon (Mai et al. 2020; Conner et al. 2021; Yusuf et al. 2022; Moreyra et al. 2023). Despite minor inconsistencies, our phylogenomic analysis of 15 species of the *Drosophila saltans* species group produced a consistent picture of the relationships between the five subgroups of this clade. All X, autosomal and mitochondrial phylogenies showed the *parasaltans* subgroup as the first to diverge, followed by the *sturtevanti* subgroup, and later by a clade comprising the *cordata*, *elliptica* and *saltans* subgroups, in which the position of the *cordata* subgroup differed between nuclear and mitochondrial trees. This general picture has not been previously proposed despite the tremendous number of phylogenetic investigations of this group (Magalhães 1962; Throckmorton 1962; Throckmorton and Magalhães 1962; O'Grady et al. 1998; Rodríguez-Trelles et al. 1999; Castro and Carareto 2004; de Setta et al. 2007; Yassin 2009; Souza et al. 2014; Roman et al. 2022; see Supplementary Table S1).

While our analysis has shed light on the intricate evolutionary dynamics within this clade, further sampling holds the potential to provide a more comprehensive understanding into this complex evolutionary history. For example, the inclusion of *D. subsaltans*, *D. lusaltans*, *D. cordata*, and *D. rectangularis* through whole-genome sequencing promises to provide insight onto unresolved phylogenetic questions raised from previously published observations on reproductive isolation and morphology (Magalhães 1962; Bicudo and Prioli 1978). These questions include the monophyly and positioning of the *parasaltans* and *cordata* subgroups. Additionally, the inclusion of the insular species *D. lusaltans* which presents low

444 reproductive isolation (Bicudo 1973b), can bring new insights into the reticulation evolution
445 in the *saltans* subgroup. The *saltans* subgroup showed the most dramatic signal of cyto-
446 nuclear discordance and reticulated evolution. Bicudo (1973b) investigated reproductive
447 isolation among the seven then described species of this subgroup, and in a remarkably partial
448 agreement with our nuclear phylogenomic trees, she concluded that *D. pseudosaltans*, *D.*
449 *nigrosaltans* and *D. austrosaltans* showed strong reproductive isolation with *D. lusaltans*, *D.*
450 *septentriosaltans*, *D. prosaltans* and *D. saltans*, *i.e.* the latter species show less reproductive
451 isolation. Indeed, nearly all crosses among the last four species produce fertile females with
452 some even producing fertile females and males (Bicudo 1973b). This behavioral porosity
453 largely agrees with the high incidence of reticulate evolution we report here for this subgroup.
454 Two widespread species of the *saltans* subgroup, *D. saltans* and *D. prosaltans*, show a
455 peculiar geographical disjunction, with the former species being restricted to Central America
456 whereas *D. prosaltans* is widespread in South America south of Costa Rica. The
457 discrimination between strains belonging to each species has long been erroneous
458 (Dobzhansky 1944; Mayr and Dobzhansky 1945; Spassky 1957; Magalhães 1962) and we
459 showed here that their misidentification persists even in the genomic era (Kim et al. 2021;
460 Suvorov, Kim, et al. 2022). Interestingly, Bicudo (1973b) provided evidence for reproductive
461 reinforcement between these two sister species; sympatric populations in their junction zone
462 in Costa Rica demonstrated stronger reproductive isolation than allopatric populations of both
463 species. We have only included one to a few geographical lines from each species and a
464 broader sampling to investigate the extent of their reproductive isolation and genome porosity
465 is strongly needed.
466
467
468

Intra- and inter-genomic conflicts impact the inference of phylogenetic patterns

Concatenation helped recovering a sex chromosome versus autosome conflict, similar to the one described by Mai et al. (2020) for the *Drosophila nasuta* subgroup. Like these authors, this conflict was limited to a single part of the tree, *i.e.* the relationship of *D. pulau* to *D. sulfurigaster sulfuricaster* and *D. s. bilimbata* in the *nasuta* subgroup and the placement of *D. lehrmanae* in the *sturtevanti* subgroup. The peculiarities of sexual chromosomes such as their lower effective population size, different recombination and mutation rates, and greater exposition to natural selection when found in hemizygosity, lead to higher rates of adaptive evolution of sexual-linked genes compared with autosomal genes (*i.e.* faster-X evolution) and also to the disproportional accumulation of genes related to reproductive isolation and Dobzhansky-Muller hybrid incompatibilities (*i.e.* Haldane's rule) (Charlesworth et al. 2018). Besides, low recombination rate underlies stronger linked selection effects against introgressed ancestry. Altogether, those characteristics are thought to be responsible for the resistance to hybridization in the sexual chromosomes (Ellegren 2009; Qvarnström and Bailey 2009; Sankararaman et al. 2016; Charlesworth et al. 2018; Seixas et al. 2018; Mai et al. 2020; Matute et al. 2020; Moran et al. 2021; Reilly et al. 2022; Skov et al. 2023; but see David et al. 2022).

The second conflict regards a significant disagreement between mitochondrial (mtDNA) and nuclear data. Discordance between nuclear and mitochondrial genomes is a well-documented phenomenon in the tree of life as highlighted by Toews and Brelsford (2012). Several characteristics of mtDNA, such as being haploid and uniparentally inherited, resulting in a fourfold reduction in effective population size when compared with autosomal loci, affect its evolution and may lead to high incidences of incomplete lineage sorting (Wang et al. 2018). An alternative explanation can be cytoplasmic introgression, which has long been recognized in *Drosophila* (Solignac et al. 1986; Ballard 2000; Llopart et al. 2014). In a recent

494 population study within the *willistoni* group, multiple mitochondrial introgressions were
495 observed in *D. paulistorum* populations (Baião et al. 2023). These included an ancient
496 introgression with a highly divergent mitochondrial type, followed by more recent events.
497 Rapid fixation of a mitochondrial type may be directly caused by a selective advantage
498 provided by the mitochondrial type itself, or indirectly facilitated by a non-selective factor,
499 such as *Wolbachia,* a bacterium known to modify the reproduction of its host (Baião et al.
500 2023). Although, interesting results have been reported from population approaches, conflicts
501 between nuclear and mitochondrial genomes have not been addressed in recent phylogenomic
502 analyses in the Drosophilidae (Mai et al. 2020; Khallaf et al. 2021; Suvorov, Kim, et al. 2022;
503 Yusuf et al. 2022). The disagreement was particularly evident for the *saltans* subgroup, where
504 it was most likely of recent origins, separating species that have diverged only 0.7 myr ago,
505 *i.e. D. nigrosaltans* and *D. pseudosaltans*. Remarkably, the two mitoclades *P* and *S* do not
506 correlate with the degree of reproductive isolation inferred by Bicudo (1973b), contrary to
507 nuclear tree, indicating that mito-nuclear conflicts in the *saltans* subgroup did not contribute
508 to the evolution of reproductive isolation in this clade.
509 Of the three subgroups for which multiple species were sequenced, the *saltans*
510 subgroup had the highest incidence of incongruences inferred by the 2A2B test. In this
511 subgroup, multiple large chromosomal inversions are known to be shared among closely-
512 related species (Dobzhansky and Pavan 1943; Cavalcanti 1948; Bicudo 1973a; Bicudo and
513 Prioli 1978) and evidence for balancing selection on ancestral inversion polymorphism has
514 been demonstrated in a number of cases (Bicudo 1973a). For example, one autosomal
515 inversion is polymorphic in *D. austrosaltans*, with one arrangement being homozygous in *D.*
516 *septentriosaltans* and *prosaltans*, and the alternative arrangement homozygous in the
517 remaining species including *D. saltans*. Such an inversion has likely been inherited from a
518 polymorphic ancestor of the *saltans* subgroup, and was maintained polymorphic in the

519 ancestor of the *septentriosaltans-prosaltans-saltans* clade before different arrangements
520 became fixed in each of these species, with one arrangement being already fixed in the
521 ancestor of the *nigrosaltans-pseudosaltans* clade. Alternatively, the inversion might have
522 originated in the ancestor of the *septentriosaltans-prosaltans-saltans* clade, then it was
523 introgressed in *D. austrosaltans*, whereas the ancestral non-inverted configuration being
524 introgressed on its own in *D. saltans*. However, this introgression scenario is less
525 parsimonious, especially given the geographical isolation of *D. saltans* from the remaining
526 species of the subgroup. Whether the high degree of incongruences in the *saltans* subgroup is
527 associated with large ancestral inversions potentially absent in other bifurcating clades would
528 require the future generation of chromosome-level assemblies for multiple *saltans* group
529 species.
530
531 *The 2A2B test on syntenic blocks helps distinguishing "soft" and "hard" introgressions*
532 Our analyses reveal that the choice of locus defining scheme can affect the degree of
533 phylogenomic uncertainty. Indeed, most studies that have provided strong evidence for
534 introgression using site-specific patterns comparisons have usually aligned reads from
535 multiple species to a single reference assembly (cf. studies compiled by Dagilis et al. 2022).
536 Whereas such an approach can increase the power (Martin et al. 2015; Pease and Hahn 2015),
537 it also introduces biases due to paralogy, misalignments or absence of collinearity among
538 species, that are now known to bias phylogenetic inference itself (Valiente-Mullor et al. 2021;
539 Rick et al. 2023). Therefore, the most common practice now is to use sets of clade-specific
540 single-copy orthologs, such as the BUSCO genes, in inferring phylogenies (Manni et al.
541 2021). Consequently, some recent introgression studies have focused on such genes. For
542 example, in a study of 155 genomes covering a wide range of drosophilid lineages, Suvorov,
543 Kim, et al. (2022) analyzed these conserved genes. While finding evidence for widespread

introgression, they also showed that their discordance estimates were highly sensitive to the length of the analyzed genes as well as by the slightest relaxation of selective pressures. We attempted here to overcome this limitation by including larger syntenic blocks, which in addition to conserved protein-coding sequences should also include presumably neutral intronic and intergenic sites. Whereas, this approach showed the lowest $|D|$, indicating that patterns predicted by introgression do not exceed 7% of the genome, it led to only 1.5-fold increase in the number of analyzed sites, most likely because our assemblies were based on only short reads. With the continuing progress in whole-chromosome sequencing techniques and assembly-to-assembly alignment tools, a better understanding of the extent of probably true or "hard" introgression events from artificial or "soft" ones may be attained.

Phyletic radiations occur when isolation barriers simultaneously and rapidly evolve between multiple populations of a species with a broad geographical or ecological breadth. Consequently, genetic lineages will be incompletely sorted in the emerging species leading to a lack of phylogenetic signals. This situation usually occurs following a rapid environmental change or expansion into a new range with new empty niches. Indeed, our historical biogeography approach shows that such situation might have favored the episodic signals of low phylogenetic signals in the *saltans* group since the episodes coincided with either the transition from wetlands into Amazonia forests in the Late Miocene or the connection of the Amazonian forest with either Central American or the Southern Atlantic forests in the Pliocene. These events have been proposed to be responsible for a wide range of rapid radiations in Neotropical taxa, such as butterflies, amphibians and birds (Batalha-Filho et al. 2013; O'Dea et al. 2016; Ledo and Colli 2017; Hoorn et al. 2022). The dating and the analyses of the extent of phylogenetic discordance in the genomes of such clades are strongly needed to identify the impact of these events on Neotropical diversification.

Materials and Methods

Sample collection, whole genome sequencing and assembly

We performed whole genome pool sequencing on female flies from 15 different species from the *saltans* group, as well as three populations of *D. sturtevanti*. The specimens used for sequencing were obtained from one or multiple strains, and detailed information regarding the number of individuals and their collection locations can be found in Supplementary Table S2. For all species, DNA extraction, PE library preparation using NEBNext Protocol, and 75x coverage double-paired Illumina Novoseq sequencing were conducted by End2End Genomics LLC, Davis, California. For all species except *D. neocordata*, we assembled the genome using the Maryland Super Read Cabog Assembler (MaSuRCA) (Zimin et al. 2013), which utilizes both the de Bruijn graph and overlap-layout-consensus (OLC) methods to generate super-reads. K-mer based genome size was estimated using KMC3 (Kokot et al. 2017) and GenomeScope v.2.0 (Ranallo-Benavidez et al. 2020). To assess the assembly's completeness, we searched for single-copy-genes (SCG) using default parameters in Busco5 (Simão et al. 2015) with the diptera_odb10 database (Kuznetsov et al. 2023). In addition to the sequenced flies, we also assembled Illumina reads the genomes of *D. saltans*, *D. neocordata*, *D. prosaltans* and *D. sturtevanti* published by Kim et al. (2021) (assembly numbers ASM1890357v1, ASM1890361v1, ASM1815127v1 and ASM1815037v1, respectively), and we used the *D. neocordata* assembly published by Baião et al. (2023) in all analyses.

Phylogenomics: Nuclear single-copy-genes

For phylogenomics analysis, SCG searches were carried out using 3,285 SCG from diptera_odb10 database inferred by Busco5 (Simão et al. 2015). SCG present in all species

were kept and aligned using the L-INS-i method implemented on MAFFT (Katoh and Standley 2013) (mafft --localpair --maxiterate 1000 –adjustdirection).

Genomic data of different species of *Drosophila* support that genes tend to be situated within the same Muller element across multiple species (see Schaeffer 2018). Taking this gene linkage into account, we reconstructed five independent datasets (Muller elements A-E), each comprising all SCG found in the respective Muller element. To achieve this, we performed a tBlastn search against the *D. melanogaster* reference genome v.6, and subsequently we concatenated genes found within the same Muller element. Phylogenetic trees were then constructed using maximum likelihood and Bayesian methods implemented in the softwares IQ-TREE (Nguyen et al. 2015) and BEAST (Bouckaert et al. 2019), respectively. A GTR + G + I substitution model was used for all analyses. An MCMC chain of 10,000,000 generations under strict clock and a Yule's model was run in BEAST followed by a 25% burnin sampling. Additionally, maximum-likelihood trees were generated for each gene, and for each Muller element, trees of corresponding genes used to reconstruct a species tree, using multi-species coalesce model implemented in ASTRAL-III (Zhang et al. 2018). Branch support was assigned using 1,000 ultrafast bootstrap in IQ-TREE (Hoang et al. 2018), posterior probability in BEAST and local posterior probability in ASTRAL-III.

Phylogenomics: Mitochondrial Genome

Mitochondrial genomes were assembled and annotated with MitoZ (Meng et al. 2019) using the Megahit assembler (Li et al. 2015). In order to ensure the exclusion of nuclear-embedded mitochondrial DNA sequences within the assembly, a strategic approach was taken. Considering that mitochondrial reads are found in higher frequency than nuclear-mitochondrial DNA sequences, the read subsampling were set to 0.5 gigabases (--data_size_for_mt_assembly 0.5). The genes obtained from the mitochondrial genome were

aligned using the MAFFT alignment tool with the --auto parameter due to the close similarity between sequences. Subsequently, the aligned genes were concatenated into a dataset for phylogenetic analysis. The concatenated dataset served as the basis for reconstructing phylogenetic trees using both Maximum Likelihood (ML) implemented in IQ-TREE and Bayesian Inference (BI) in BEAST. A GTR + G + I + F substitution model, inferred by IQ-TREE, was used for all analyses. An MCMC chain of 10,000,000 generations under relaxed clock and a Yule's model was run in BEAST followed by a 25% burnin sampling. Branch support was assigned using 1,000 ultrafast bootstrap in IQ-TREE and posterior probability in BEAST.

Identification of syntenic blocks

The 20 genomes of the *saltans* group, the 15 sequenced here and the 5 published by Kim et al. (2021) and Baião et al. (2023) were preliminary annotated with Miniprot (miniprot -Iut16, Li 2023). The primary objective of this annotation was to accurately map proteins from the robust and reliable genome annotation of *D. willistoni* (Clark et al. 2007). After protein mapping, the predicted gene loci were assessed to identify syntenic blocks present in the Neotropical *Sophophora* (comprising *D. willistoni* and *saltans* group). The identification of these blocks was based on gene order and orientation, achieved using an in-house Perl script. First, this script compares the scaffolds' genes order and orientation between the reference assemblies of *D. saltans* and *D. sturtevanti*, the synteny blocks were defined when all the genes were found in the same order and orientation in both species. The identified collinear blocks were then searched for the remaining genomes including the *D. willistoni* genome. Blocks with missing data, *i.e.* missing genes for one or more species were subsequently removed, and the remaining blocks were subjected to a size-based filtering with a threshold of ≥50kb. The selected blocks were aligned using the Mafft software (Katoh and Standley 2013).

644

645 *Pseudo-reference inference*

646 Illumina reads were aligned on either the *D. willistoni* reference genome (Clark et al.
647 2007: 12) or the recently published *D. sturtevanti* assembly (Kim et al. 2021) using minimap2
648 (Li 2018). Minimap2 generated BAM files were assembled into a pseudo-reference for each
649 species using the BCFtools software (Danecek et al. 2021). We did not first apply any
650 mapping quality criteria. For subsequent analyses, we only retained homozygous sites with
651 mapping quality >20 and a depth >10 and <100. Each scaffold was then split into 100 kb-long
652 windows.

653

654 *Quantifying reticulation using the 2A2B test*

655 Combinations of 28 species quartets were evaluated to test reticulation, bi-allelic sited
656 shared by pairs were searched in every locus, whether using BUSCO, syntenic blocks or
657 pseudo-reference 100 kb-long windows. Loci with at least 20 informative sites were retained.
658 To reduce the influence of loci with higher number of evaluated sites, we concatenated
659 randomly drawn 20 sites from each locus. We then estimated Patterson's *D*, *i.e.* (∑ABBA –
660 ∑BABA)/(∑ABBA + ∑BABA), as an average of 100 iterations of this random sampling for
661 each quartet. To account for cases where a true species may not be present, we devised a new
662 test that we called 2A2B. For each locus or to the concatenated sequences constructed as
663 above, the occurrences BBAA, ABBA or BABA patterns were counted, and three pairwise χ^2-
664 based tests were conducted, denoted *D1*, *D2*, and *D3* as follows (D1 is similar to Patterson's
665 D):

666 $$D1 = (\sum ABBA - \sum BABA)^2/(\sum ABBA + \sum BABA),$$

667 $$D2 = (\sum BBAA - \sum ABBA)^2/(\sum BBAA + \sum ABBA), \text{ and}$$

668 $$D3 = (\sum BBAA - \sum BABA)^2/(\sum BBAA + \sum BABA).$$

669 Each of these estimates is reminiscent to the classical Tajima's (1993) Relative Rate Test
670 (RTT), which tests the molecular clock hypothesis as difference in branch lengths from two
671 ingroup taxa to a third outgroup taxon, with lengths estimated as counts of different sites.
672 However, unlike RRT, branch lengths in our analyses are counted in terms of shared
673 differences, *i.e.* singletons are not considered. Similar to RRT, we applied a chi-squared
674 analysis to test for deviation from parity for each parameter. According to the significance
675 levels of the three estimates, a locus can be classified under each of the four categories
676 presented in Figure 1. The test is run by the 2A2B perl script associated with this manuscript.
677 To test molecular clock in our analyses, which can bias incongruence inference (Frankel and
678 Ané 2023), we also applied a quartet-adapted version of the RRT that we called 3A1B test,
679 wherein sites with singletons (BBBA, ABAA and BAAA) were also counted and loci
680 violating the assumption of BBBA – ABAA and BBBA – BAAA > 0 were excluded from the
681 analyses. For pseudo-reference approaches, only sites that were mapped on the reference
682 genomes were evaluated, *i.e.* any missing site of any species was not evaluated in the quartet
683 including that species.
684
685 *Historical biogeography*
686 To determine the sampling locations of the evaluated species, we parsed coordinates of
687 current distribution of the studied species obtained from TaxoDros
688 (https://www.taxodros.uzh.ch/search/class.php). Additionally, we incorporated sampling sites
689 that we ourselves had conducted. The accuracy of our species identification was previously
690 confirmed through DNA barcoding. After inspection of the geographical points and manual
691 correction, we identified the most northern, southern, western, and eastern points for each
692 species. We used those points to reconstruct the ancestral geographical range by conducting a
693 BayesTraits (Meade and Pagel 2022) analysis for each cartesian point separately. The

694 analyses were carried out using the GEO model with the phylogenetic tree generated
695 reconstructed with the Muller element A (XL chromosome arm) after 1,000,000 MCMC
696 iterations and 25% burn-in. The divergence times were estimated using this tree under
697 Bayesian inference. The calibration point used was the split between *D. willistoni* and *D.*
698 *sturtevanti* at 17.5 myr, as estimated by Suvorov, Kim, et al. (2022). To visualize the
699 biogeographical history, we plotted the inferred centroid coordinates, *i.e.* averaged latitudes
700 and longitudes of the four extreme points, for each terminal and internal node on the map of
701 Central and South Americas using the maps v.3.4.2.1 software package (Deckmyn 2024) in R
702 (R Core Team 2023).

References

Bächli G. 2024. TaxoDros: the database on Taxonomy of Drosophilidae. Available from: https://www.taxodros.uzh.ch/

Baião GC, Schneider DI, Miller WJ, Klasson L. 2023. Multiple introgressions shape mitochondrial evolutionary history in *Drosophila paulistorum* and the *Drosophila willistoni* group. *Molecular Phylogenetics and Evolution* 180:107683.

Ballard JWO. 2000. Comparative Genomics of Mitochondrial DNA in Members of the Drosophila melanogaster Subgroup. *J Mol Evol* 51:48–63.

Batalha-Filho H, Fjeldså J, Fabre P-H, Miyaki CY. 2013. Connections between the Atlantic and the Amazonian forest avifaunas represent distinct historical events. *J Ornithol* 154:41–50.

Bicudo HEMC. 1973a. Chromosomal polymorphism in the saltans group of Drosophila I. The saltans subgroup. *Genetica* 44:520–552.

Bicudo HEMC. 1973b. Reproductive isolation in the saltans group of Drosophila. I. The saltans subgroup. *Genetica* 44:313–329.

Bicudo HEMC. 1979. Reproductive isolation of the saltans group of Drosophila. IV. the sturtevanti subgroup. *Revista Brasileira de Genética* 2:247–258.

Bicudo HEMC, Prioli AJ. 1978. Reproductive isolation in the saltans group of Drosophila II. The parasaltans subgroup. *Genetica* 48:17–22.

Blischak PD, Chifman J, Wolfe AD, Kubatko LS. 2018. HyDe: A Python Package for Genome-Scale Hybridization Detection. *Systematic Biology* 67:821–829.

Bouckaert R, Vaughan TG, Barido-Sottani J, Duchêne S, Fourment M, Gavryushkina A, Heled J, Jones G, Kühnert D, Maio ND, et al. 2019. BEAST 2.5: An advanced software platform for Bayesian evolutionary analysis. *PLOS Computational Biology* 15:e1006650.

Camacho C, Coulouris G, Avagyan V, Ma N, Papadopoulos J, Bealer K, Madden TL. 2009. BLAST+: architecture and applications. *BMC Bioinformatics* 10:421.

728 Castro JP de, Carareto CMA. 2004. *P* elements in the *saltans* group of *Drosophila*: a new
729 evaluation of their distribution and number of genomic insertion sites. *Molecular Phylogenetics*
730 *and Evolution* 32:383–387.
731 Cavalcanti AGL. 1948. Geographic Variation of Chromosome Structure in Drosophila
732 Prosaltans. *Genetics* 33:529–536.
733 Chang ES, Neuhof M, Rubinstein ND, Diamant A, Philippe H, Huchon D, Cartwright P. 2015.
734 Genomic insights into the evolutionary origin of Myxozoa within Cnidaria. *Proceedings of the*
735 *National Academy of Sciences* 112:14912–14917.
736 Charlesworth B, Campos JL, Jackson BC. 2018. Faster-X evolution: Theory and evidence from
737 Drosophila. *Molecular Ecology* 27:3753–3771.
738 Clark AG, Eisen MB, Smith DR, Bergman CM, Oliver B, Markow TA, Kaufman TC, Kellis
739 M, Gelbart W, Iyer VN, et al. 2007. Evolution of genes and genomes on the Drosophila
740 phylogeny. *Nature* 450:203–218.
741 Conner WR, Delaney EK, Bronski MJ, Ginsberg PS, Wheeler TB, Richardson KM,
742 Peckenpaugh B, Kim KJ, Watada M, Hoffmann AA, et al. 2021. A phylogeny for the
743 *Drosophila montium* species group: A model clade for comparative analyses. *Molecular*
744 *Phylogenetics and Evolution* 158:107061.
745 Dagilis AJ, Peede D, Coughlan JM, Jofre GI, D'Agostino ERR, Mavengere H, Tate AD, Matute
746 DR. 2022. A need for standardized reporting of introgression: Insights from studies across
747 eukaryotes. *Evolution Letters* 6:344–357.
748 Danecek P, Bonfield JK, Liddle J, Marshall J, Ohan V, Pollard MO, Whitwham A, Keane T,
749 McCarthy SA, Davies RM, et al. 2021. Twelve years of SAMtools and BCFtools. *GigaScience*
750 10:giab008.
751 David JR, Ferreira EA, Jabaud L, Ogereau D, Bastide H, Yassin A. 2022. Evolution of
752 assortative mating following selective introgression of pigmentation genes between two

753 Drosophila species. *Ecology and Evolution* 12:e8821.
754 Deckmyn OS code by RAB and ARWR version by RBE by TPM and A. 2024. maps: Draw
755 Geographical Maps. Available from: https://cran.r-project.org/web/packages/maps/index.html
756 Dobzhansky TG, Pavan C. 1943. Studies on Brazilian species of Drosophila. *Boletim da*
757 *Faculdade de Filosofia, Ciências e Letras da Universidade de São Paulo. Biologia Geral.*
758 *Separata* 36:7–72.
759 Dobzhansky Th. 1944. Experiments on Sexual Isolation in Drosophila. *Proceedings of the*
760 *National Academy of Sciences* 30:335–339.
761 Doronina L, Churakov G, Shi J, Brosius J, Baertsch R, Clawson H, Schmitz J. 2015. Exploring
762 Massive Incomplete Lineage Sorting in Arctoids (Laurasiatheria, Carnivora). *Molecular*
763 *Biology and Evolution* 32:3194–3204.
764 Durand EY, Patterson N, Reich D, Slatkin M. 2011. Testing for Ancient Admixture between
765 Closely Related Populations. *Molecular Biology and Evolution* 28:2239–2252.
766 Ellegren H. 2009. The different levels of genetic diversity in sex chromosomes and autosomes.
767 *Trends in Genetics* 25:278–284.
768 Frankel LE, Ané C. 2023. Summary Tests of Introgression Are Highly Sensitive to Rate
769 Variation Across Lineages. *Systematic Biology* 72:1357–1369.
770 Gagnon E, Hilgenhof R, Orejuela A, McDonnell A, Sablok G, Aubriot X, Giacomin L, Gouvêa
771 Y, Bragionis T, Stehmann JR, et al. 2022. Phylogenomic discordance suggests polytomies
772 along the backbone of the large genus Solanum. *American Journal of Botany* 109:580–601.
773 Glor RE. 2010. Phylogenetic Insights on Adaptive Radiation. *Annual Review of Ecology,*
774 *Evolution, and Systematics* 41:251–270.
775 Green RE, Krause J, Briggs AW, Maricic T, Stenzel U, Kircher M, Patterson N, Li H, Zhai W,
776 Fritz MH-Y, et al. 2010. A Draft Sequence of the Neandertal Genome. *Science* 328:710–722.
777 Hibbins MS, Hahn MW. 2022. Phylogenomic approaches to detecting and characterizing

introgression. *Genetics* 220:iyab173.

Hime PM, Lemmon AR, Lemmon ECM, Prendini E, Brown JM, Thomson RC, Kratovil JD, Noonan BP, Pyron RA, Peloso PLV, et al. 2021. Phylogenomics Reveals Ancient Gene Tree Discordance in the Amphibian Tree of Life. *Systematic Biology* 70:49–66.

Hoang DT, Chernomor O, von Haeseler A, Minh BQ, Vinh LS. 2018. UFBoot2: Improving the Ultrafast Bootstrap Approximation. *Molecular Biology and Evolution* 35:518–522.

Hoorn C, Boschman LM, Kukla T, Sciumbata M, Val P. 2022. The Miocene wetland of western Amazonia and its role in Neotropical biogeography. *Botanical Journal of the Linnean Society* 199:25–35.

Jiang X, Edwards SV, Liu L. 2020. The Multispecies Coalescent Model Outperforms Concatenation Across Diverse Phylogenomic Data Sets. *Systematic Biology* 69:795–812.

Katoh K, Standley DM. 2013. MAFFT Multiple Sequence Alignment Software Version 7: Improvements in Performance and Usability. *Molecular Biology and Evolution* 30:772–780.

Khallaf MA, Cui R, Weißflog J, Erdogmus M, Svatoš A, Dweck HKM, Valenzano DR, Hansson BS, Knaden M. 2021. Large-scale characterization of sex pheromone communication systems in Drosophila. *Nat Commun* 12:4165.

Kim BY, Wang JR, Miller DE, Barmina O, Delaney E, Thompson A, Comeault AA, Peede D, D'Agostino ER, Pelaez J, et al. 2021. Highly contiguous assemblies of 101 drosophilid genomes.Coop G, Wittkopp PJ, Sackton TB, editors. *eLife* 10:e66405.

Kokot M, Długosz M, Deorowicz S. 2017. KMC 3: counting and manipulating k-mer statistics. *Bioinformatics* 33:2759–2761.

Kuznetsov D, Tegenfeldt F, Manni M, Seppey M, Berkeley M, Kriventseva EV, Zdobnov EM. 2023. OrthoDB v11: annotation of orthologs in the widest sampling of organismal diversity. *Nucleic Acids Research* 51:D445–D451.

Ledo RMD, Colli GR. 2017. The historical connections between the Amazon and the Atlantic

803 Forest revisited. *Journal of Biogeography* 44:2551–2563.
804 Li D, Liu C-M, Luo R, Sadakane K, Lam T-W. 2015. MEGAHIT: an ultra-fast single-node
805 solution for large and complex metagenomics assembly via succinct de Bruijn graph.
806 *Bioinformatics* 31:1674–1676.
807 Li F, Rane RV, Luria V, Xiong Z, Chen J, Li Z, Catullo RA, Griffin PC, Schiffer M, Pearce S,
808 et al. 2022. Phylogenomic analyses of the genus Drosophila reveals genomic signals of climate
809 adaptation. *Molecular Ecology Resources* 22:1559–1581.
810 Li H. 2018. Minimap2: pairwise alignment for nucleotide sequences. *Bioinformatics* 34:3094–
811 3100.
812 Li H. 2023. Protein-to-genome alignment with miniprot. *Bioinformatics* 39:btad014.
813 Lin M-J, Iyer S, Chen N-C, Langmead B. 2024. Measuring, visualizing, and diagnosing
814 reference bias with biastools. *Genome Biology* 25:101.
815 Lipman DJ, Souvorov A, Koonin EV, Panchenko AR, Tatusova TA. 2002. The relationship of
816 protein conservation and sequence length. *BMC Evolutionary Biology*.
817 Llopart A, Herrig D, Brud E, Stecklein Z. 2014. Sequential adaptive introgression of the
818 mitochondrial genome in Drosophila yakuba and Drosophila santomea. *Molecular Ecology*
819 23:1124–1136.
820 Maddison W. 1989. Reconstructing Character Evolution on Polytomous Cladograms.
821 *Cladistics* 5:365–377.
822 Maddison WP. 1997. Gene Trees in Species Trees. *Systematic Biology* 46:523–536.
823 Madi-Ravazzi L, Segala LF, Roman BE, Alevi KCC, Prediger C, Yassin A, Hua-VAN AL,
824 Miller WJ. 2021. Integrative taxonomy and a new species description in the sturtevanti
825 subgroup of the Drosophila saltans group (Diptera: Drosophilidae). *Zootaxa* 4980:269292.
826 Magalhães LE de. 1962. Notes on the taxonomy, morphology, and distribution of the saltans
827 group of Drosophila, with descriptions of four new species. *The University of Texas Publication*

828 2:135–154.
829 Magalhães LE de, Björnberg AJS. 1957. Estudo da genitália masculina de “Drosophila” do
830 grupo “saltans” (Diptera). *Revista Brasileira de Biologia* 17:435–450.
831 Mai D, Nalley MJ, Bachtrog D. 2020. Patterns of Genomic Differentiation in the Drosophila
832 nasuta Species Complex. *Molecular Biology and Evolution* 37:208–220.
833 Malinsky M, Matschiner M, Svardal H. 2021. Dsuite - Fast D-statistics and related admixture
834 evidence from VCF files. *Molecular Ecology Resources* 21:584–595.
835 Manni M, Berkeley MR, Seppey M, Zdobnov EM. 2021. BUSCO: Assessing Genomic Data
836 Quality and Beyond. *Current Protocols* 1:e323.
837 Martin SH, Davey JW, Jiggins CD. 2015. Evaluating the Use of ABBA–BABA Statistics to
838 Locate Introgressed Loci. *Molecular Biology and Evolution* 32:244–257.
839 Matute DR, Comeault AA, Earley E, Serrato-Capuchina A, Peede D, Monroy-Eklund A, Huang
840 W, Jones CD, Mackay TFC, Coyne JA. 2020. Rapid and Predictable Evolution of Admixed
841 Populations Between Two Drosophila Species Pairs. *Genetics* 214:211–230.
842 Mayr E, Dobzhansky Th. 1945. Experiments on Sexual Isolation in Drosophila. *Proceedings of*
843 *the National Academy of Sciences* 31:75–82.
844 Meade A, Pagel M. 2022. Ancestral State Reconstruction Using BayesTraits. In: Luo H, editor.
845 Environmental Microbial Evolution: Methods and Protocols. Methods in Molecular Biology.
846 New York, NY: Springer US. p. 255–266. Available from: https://doi.org/10.1007/978-1-0716-
847 2691-7_12
848 Meng G, Li Y, Yang C, Liu S. 2019. MitoZ: a toolkit for animal mitochondrial genome
849 assembly, annotation and visualization. *Nucleic Acids Research* 47:e63.
850 Minh BQ, Schmidt HA, Chernomor O, Schrempf D, Woodhams MD, von Haeseler A, Lanfear
851 R. 2020. IQ-TREE 2: New Models and Efficient Methods for Phylogenetic Inference in the
852 Genomic Era. *Molecular Biology and Evolution* 37:1530–1534.

853 Moran BM, Payne C, Langdon Q, Powell DL, Brandvain Y, Schumer M. 2021. The genomic
854 consequences of hybridization.Wittkopp PJ, editor. *eLife* 10:e69016.
855 Moreyra NN, Almeida FC, Allan C, Frankel N, Matzkin LM, Hasson E. 2023. Phylogenomics
856 provides insights into the evolution of cactophily and host plant shifts in *Drosophila*. *Molecular*
857 *Phylogenetics and Evolution* 178:107653.
858 Morgan CC, Foster PG, Webb AE, Pisani D, McInerney JO, O'Connell MJ. 2013.
859 Heterogeneous Models Place the Root of the Placental Mammal Phylogeny. *Molecular Biology*
860 *and Evolution* 30:2145–2156.
861 Nascimento AP, Bicudo HEMC. 2002. Esterase Patterns and Phylogenetic Relationships of
862 Drosophila Species in the Saltans Subgroup (Saltans Group). *Genetica* 114:41–51.
863 Nguyen L-T, Schmidt HA, von Haeseler A, Minh BQ. 2015. IQ-TREE: A Fast and Effective
864 Stochastic Algorithm for Estimating Maximum-Likelihood Phylogenies. *Molecular Biology*
865 *and Evolution* 32:268–274.
866 O'Dea A, Lessios HA, Coates AG, Eytan RI, Restrepo-Moreno SA, Cione AL, Collins LS, de
867 Queiroz A, Farris DW, Norris RD, et al. 2016. Formation of the Isthmus of Panama. *Science*
868 *Advances* 2:e1600883.
869 O'Grady PM, Clark JB, Kidwell MG. 1998. Phylogeny of the Drosophila saltans species group
870 based on combined analysis of nuclear and mitochondrial DNA sequences. *Molecular Biology*
871 *and Evolution* 15:656–664.
872 Owen CL, Miller GL. 2022. Phylogenomics of the Aphididae: Deep relationships between
873 subfamilies clouded by gene tree discordance, introgression and the gene tree anomaly zone.
874 *Systematic Entomology* 47:470–486.
875 Pease JB, Hahn MW. 2015. Detection and Polarization of Introgression in a Five-Taxon
876 Phylogeny. *Systematic Biology* 64:651–662.
877 Pélandakis M, Solignac M. 1993. Molecular phylogeny of Drosophila based on ribosomal RNA

878 sequences. *J Mol Evol* 37:525–543.
879 Philippe H, Brinkmann H, Lavrov DV, Littlewood DTJ, Manuel M, Wörheide G, Baurain D.
880 2011. Resolving Difficult Phylogenetic Questions: Why More Sequences Are Not Enough.
881 *PLOS Biology* 9:e1000602.
882 Philippe H, Derelle R, Lopez P, Pick K, Borchiellini C, Boury-Esnault N, Vacelet J, Renard E,
883 Houliston E, Quéinnec E, et al. 2009. Phylogenomics Revives Traditional Views on Deep
884 Animal Relationships. *Current Biology* 19:706–712.
885 Pick KS, Philippe H, Schreiber F, Erpenbeck D, Jackson DJ, Wrede P, Wiens M, Alié A,
886 Morgenstern B, Manuel M, et al. 2010. Improved Phylogenomic Taxon Sampling Noticeably
887 Affects Nonbilaterian Relationships. *Molecular Biology and Evolution* 27:1983–1987.
888 Quintero I, Keil P, Jetz W, Crawford FW. 2015. Historical Biogeography Using Species
889 Geographical Ranges. *Systematic Biology* 64:1059–1073.
890 Qvarnström A, Bailey RI. 2009. Speciation through evolution of sex-linked genes. *Heredity*
891 102:4–15.
892 R Core Team. 2023. R: A Language and Environment for Statistical Computing. Available
893 from: https://www.R-project.org/
894 Ranallo-Benavidez TR, Jaron KS, Schatz MC. 2020. GenomeScope 2.0 and Smudgeplot for
895 reference-free profiling of polyploid genomes. *Nat Commun* 11:1432.
896 Reilly PF, Tjahjadi A, Miller SL, Akey JM, Tucci S. 2022. The contribution of Neanderthal
897 introgression to modern human traits. *Current Biology* 32:R970–R983.
898 Rick JA, Brock CD, Lewanski AL, Golcher-Benavides J, Wagner CE. 2023. Reference Genome
899 Choice and Filtering Thresholds Jointly Influence Phylogenomic Analyses. *Systematic*
900 *Biology*:syad065.
901 Rodríguez-Trelles F, Tarrío R, Ayala FJ. 1999. Molecular Evolution and Phylogeny of the
902 *Drosophila saltans* Species Group Inferred from the *Xdh* Gene. *Molecular Phylogenetics and*

903 *Evolution* 13:110–121.
904 Roman BE, Madi-Ravazzi L. 2021. Male terminalia morphology of sixteen species of the
905 Drosophila saltans group Sturtevant (Diptera, Drosophilidae). *Zootaxa* 5061:523–544.
906 Roman BE, Santana DJ, Prediger C, Madi-Ravazzi L. 2022. Phylogeny of Drosophila saltans
907 group (Diptera: Drosophilidae) based on morphological and molecular evidence. *PLOS ONE*
908 17:e0266710.
909 Romiguier J, Ranwez V, Delsuc F, Galtier N, Douzery EJP. 2013. Less Is More in Mammalian
910 Phylogenomics: AT-Rich Genes Minimize Tree Conflicts and Unravel the Root of Placental
911 Mammals. *Molecular Biology and Evolution* 30:2134–2144.
912 Ronquist F, Teslenko M, van der Mark P, Ayres DL, Darling A, Höhna S, Larget B, Liu L,
913 Suchard MA, Huelsenbeck JP. 2012. MrBayes 3.2: Efficient Bayesian Phylogenetic Inference
914 and Model Choice Across a Large Model Space. *Systematic Biology* 61:539–542.
915 Sankararaman S, Mallick S, Patterson N, Reich D. 2016. The Combined Landscape of
916 Denisovan and Neanderthal Ancestry in Present-Day Humans. *Current Biology* 26:1241–1247.
917 Sarver BAJ, Keeble S, Cosart T, Tucker PK, Dean MD, Good JM. 2017. Phylogenomic Insights
918 into Mouse Evolution Using a Pseudoreference Approach. *Genome Biology and Evolution*
919 9:726–739.
920 Sayyari E, Mirarab S. 2018. Testing for Polytomies in Phylogenetic Species Trees Using
921 Quartet Frequencies. *Genes* 9:132.
922 Schaeffer SW. 2018. Muller "Elements" in Drosophila: How the Search for the Genetic Basis
923 for Speciation Led to the Birth of Comparative Genomics. *Genetics* 210:3–13.
924 Schrempf D, Szöllősi G. 2020. The Sources of Phylogenetic Conflicts. In: No commercial
925 publisher | Authors open access book. p. 3.1:1. Available from: https://hal.science/hal-
926 02535482
927 Seixas FA, Boursot P, Melo-Ferreira J. 2018. The genomic impact of historical hybridization

928 with massive mitochondrial DNA introgression. *Genome Biology* 19:91.
929 de Setta N, Loreto ELS, Carareto CMA. 2007. Is the Evolutionary History of the O-Type P
930 Element in the saltans and willistoni Groups of Drosophila Similar to That of the Canonical P
931 Element? *J Mol Evol* 65:715–724.
932 Simão FA, Waterhouse RM, Ioannidis P, Kriventseva EV, Zdobnov EM. 2015. BUSCO:
933 assessing genome assembly and annotation completeness with single-copy orthologs.
934 *Bioinformatics* 31:3210–3212.
935 Simion P, Philippe H, Baurain D, Jager M, Richter DJ, Di Franco A, Roure B, Satoh N,
936 Quéinnec É, Ereskovsky A, et al. 2017. A Large and Consistent Phylogenomic Dataset Supports
937 Sponges as the Sister Group to All Other Animals. *Current Biology* 27:958–967.
938 Skov L, Coll Macià M, Lucotte EA, Cavassim MIA, Castellano D, Schierup MH, Munch K.
939 2023. Extraordinary selection on the human X chromosome associated with archaic admixture.
940 *Cell Genomics* 3:100274.
941 Solignac M, Monnerot M, Mounolou J-C. 1986. Mitochondrial DNA evolution in
942 themelanogaster species subgroup ofDrosophila. *J Mol Evol* 23:31–40.
943 Souza TAJ, Noll FB, Bicudo HEMC, Madi-Ravazzi L. 2014. Scanning Electron Microscopy
944 of Male Terminalia and Its Application to Species Recognition and Phylogenetic
945 Reconstruction in the Drosophila saltans Group. *PLOS ONE* 9:e97156.
946 Spassky B. 1957. Morphological differences between sibling species of Drosophila. *University*
947 *of Texas Publication* 5721:48–61.
948 Sturtevant AH. 1942. The classification of the genus Drosophila, with descriptions of nine
949 species. *University of Texas Publication* 4213:5–51.
950 Sturtevant AH, Novitski E. 1941. THE HOMOLOGIES OF THE CHROMOSOME
951 ELEMENTS IN THE GENUS DROSOPHILA. *Genetics* 26:517–541.
952 Suh A. 2016. The phylogenomic forest of bird trees contains a hard polytomy at the root of

953 Neoaves. *Zoologica Scripta* 45:50–62.
954 Suvorov A, Kim BY, Wang J, Armstrong EE, Peede D, D'Agostino ERR, Price DK, Waddell
955 PJ, Lang M, Courtier-Orgogozo V, et al. 2022. Widespread introgression across a phylogeny
956 of 155 *Drosophila* genomes. *Current Biology* 32:111-123.e5.
957 Suvorov A, Scornavacca C, Fujimoto MS, Bodily P, Clement M, Crandall KA, Whiting MF,
958 Schrider DR, Bybee SM. 2022. Deep Ancestral Introgression Shapes Evolutionary History of
959 Dragonflies and Damselflies. *Systematic Biology* 71:526–546.
960 Tajima F. 1993. Simple methods for testing the molecular evolutionary clock hypothesis.
961 *Genetics* 135:599–607.
962 Throckmorton LH. 1962. The problem of phylogeny in the genus Drosophila.Studies in
963 Genetics.II. *University of Texas Publication* 6205:207–343.
964 Throckmorton LH, Magalhães LE de. 1962. Changes with evolution of pteridine accumulations
965 in species of the saltans group of the genus Drosophila. *University of Texas Publication*
966 6205:489–505.
967 Toews DPL, Brelsford A. 2012. The biogeography of mitochondrial and nuclear discordance
968 in animals. *Molecular Ecology* 21:3907–3930.
969 Townsend JP, Su Z, Tekle YI. 2012. Phylogenetic Signal and Noise: Predicting the Power of a
970 Data Set to Resolve Phylogeny. *Systematic Biology* 61:835.
971 Valiente-Mullor C, Beamud B, Ansari I, Francés-Cuesta C, García-González N, Mejía L, Ruiz-
972 Hueso P, González-Candelas F. 2021. One is not enough: On the effects of reference genome
973 for the mapping and subsequent analyses of short-reads. *PLOS Computational Biology*
974 17:e1008678.
975 Walsh HE, Kidd MG, Moum T, Friesen VL. 1999. Polytomies and the Power of Phylogenetic
976 Inference. *Evolution* 53:932–937.
977 Wang K, Lenstra JA, Liu L, Hu Q, Ma T, Qiu Q, Liu J. 2018. Incomplete lineage sorting rather

978 than hybridization explains the inconsistent phylogeny of the wisent. *Commun Biol* 1:169.
979 Whelan NV, Kocot KM, Moroz LL, Halanych KM. 2015. Error, signal, and the placement of
980 Ctenophora sister to all other animals. *Proceedings of the National Academy of Sciences*
981 112:5773–5778.
982 Wickett NJ, Mirarab S, Nguyen N, Warnow T, Carpenter E, Matasci N, Ayyampalayam S,
983 Barker MS, Burleigh JG, Gitzendanner MA, et al. 2014. Phylotranscriptomic analysis of the
984 origin and early diversification of land plants. *Proceedings of the National Academy of Sciences*
985 111:E4859–E4868.
986 Yassin A. 2009. Phylogenetic relationships among species subgroups in the Drosophila saltans
987 group (Diptera: Drosophilidae): Can morphology solve a molecular conflict. *Zool Res* 30:225–
988 232.
989 Yusuf LH, Tyukmaeva V, Hoikkala A, Ritchie MG. 2022. Divergence and introgression among
990 the virilis group of Drosophila. *Evolution Letters* 6:537–551.
991 Zhang C, Rabiee M, Sayyari E, Mirarab S. 2018. ASTRAL-III: polynomial time species tree
992 reconstruction from partially resolved gene trees. *BMC Bioinformatics* 19:153.
993 Zimin AV, Marçais G, Puiu D, Roberts M, Salzberg SL, Yorke JA. 2013. The MaSuRCA
994 genome assembler. *Bioinformatics* 29:2669–2677.
995

996 **Figure legends**

997

998 **Figure 1 –** The distribution of bi-allelic sites proportions among three ingroup species with an
999 outgroup and the rationale of the 2A2B test. A) Statistical pairwise comparisons of the three
1000 possible bi-allelic patterns generate four categories. B) Each category corresponds to a
1001 possible evolutionary scenario along a phylogenetic resolution continuum: (i) complete
1002 trifurcation, (ii) incomplete trifurcation, (iii) incomplete bifurcation, and (iv) complete
1003 bifurcation. Categories ii and iii correspond to cases of reticulate evolution. The 2A2B test
1004 estimates significant deviation from parity in pairwise comparisons of the topologies. *:
1005 significant deviation, n.s. = non-significant.

1006

1007 **Figure 2 –** Phylogenomic conflict between the X chromosome, autosomes, and the
1008 mitochondria. A) Comparison of autosomal topology (left, represented by Muller element B)
1009 and X chromosome topology (right, represented by Muller element A) demonstrates overall
1010 agreement with minor incongruence. B) Mitochondrial-nuclear disagreement highlights
1011 stronger incongruence between mitochondrial topology (left) and X chromosome topology
1012 (right, same as above but after midpoint rooting). All trees were inferred through Bayesian
1013 analysis. Divergence time estimation (in million years ago, myr) for the X chromosome
1014 topology is provided (left). Nodes are numbered for subsequent analyses. Maximum-
1015 likelihood and ASTRAL-III trees are provided in Supplementary Figures S2 and S3,
1016 respectively. Posterior probabilities (PP) of all nodes were equal to 1, except for nodes
1017 indicated with a blank circle where PP were equal to 0.87.

1018

1019 **Figure 3 –** Extent of phylogenomic discordance using four locus-definition strategies (see
1020 text) as measured by Patterson's *D* on a concatenated sequence of 20 randomly selected bi-

allelic sites per locus, across 28 species quartets A) before and B) after correction for molecular clock (assembly-based approaches) and mapping quality (pseudo-reference approaches).

Figure 4 – The 2A2B test using four locus-definition strategies (see text) across 28 species quartets as measured on a concatenated sequence of 20 randomly selected bi-allelic sites per locus after correction for molecular clock (assembly-based approaches) and mapping quality (pseudo-reference approaches). Colors of bars correspond to the four categories presented in Figure 1.

Figure 5 – Historical biogeography of the *saltans* species group showing correspondence between episodes of rapid radiation and paleogeographical events. Centroid geographical coordinates for each species were inferred and ancestral coordinates were estimated using BayesTraits on the Bayesian X chromosome chronogram given in Figure 2B. Terminal and internal nodes coordinates are projected on the current map of South and Central America as dots with their labels and colors similar to Figure 2B. Age ranges are given for internal nodes grouped by dotted contours showing the association between the split of A) the five subgroups and the formation of the Amazonian river around 10 myr ago, B) of the *sturtevanti* subgroup species and the connection between the Amazonian and Atlantic rainforests around 2.5 myr ago, and C) of the *elliptica* and D) the *saltans* subgroups species and the formation of the isthmus of Panama around 3 myr ago. Photos of adult males of four representative species are shown.

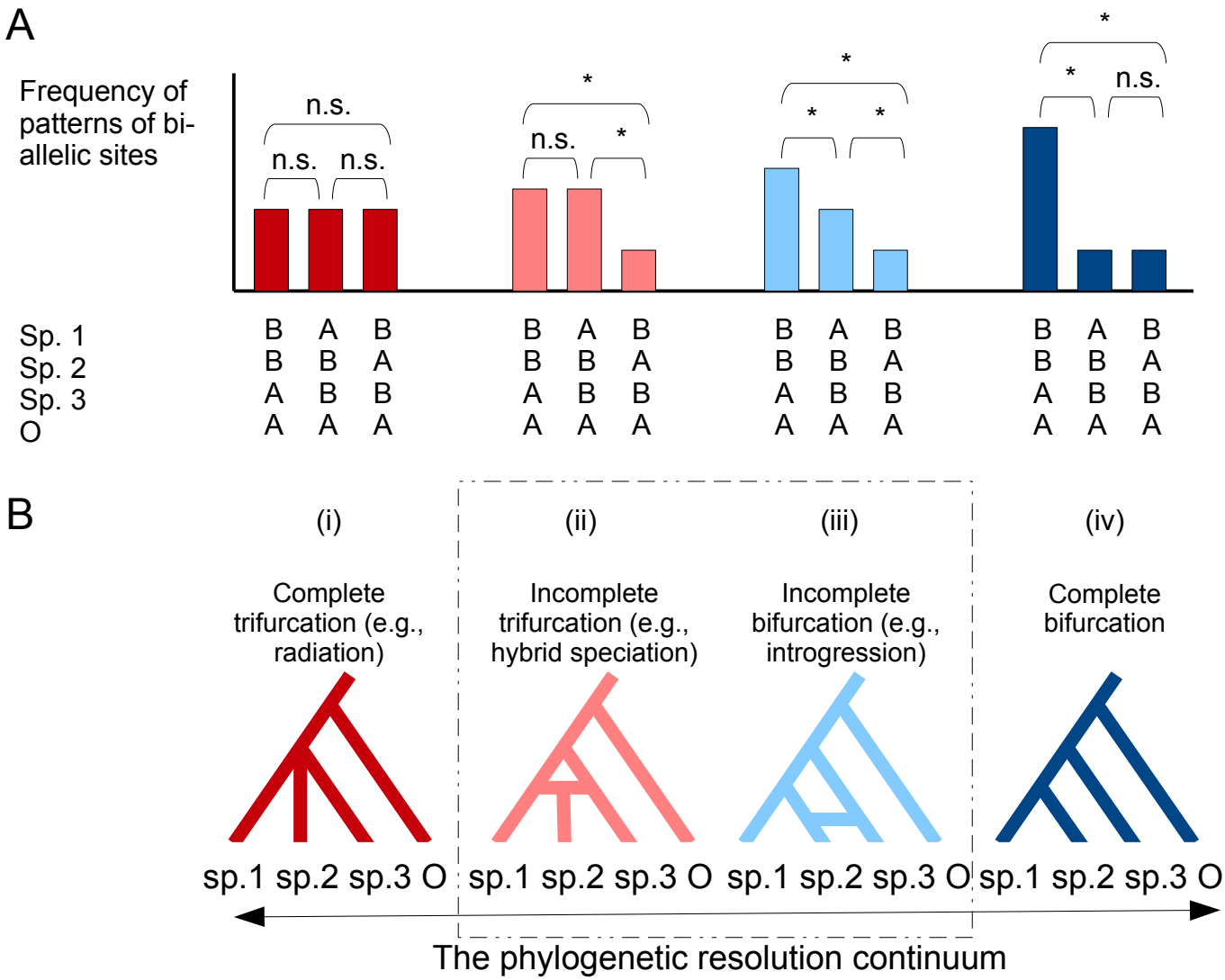
A
Frequency of patterns of bi-allelic sites
n.s.
n.s.
n.s.
*
n.s.
*
*
*
*
*
*
n.s.
Sp. 1
Sp. 2
Sp. 3
O
B B A A
A B B A
B A B A
B A A A
B
(i)
(ii)
(iii)
(iv)
Complete trifurcation (e.g., radiation)
Incomplete trifurcation (e.g., hybrid speciation)
Incomplete bifurcation (e.g., introgression)
Complete bifurcation
sp.1 sp.2 sp.3 O
The phylogenetic resolution continuum

Figure 1

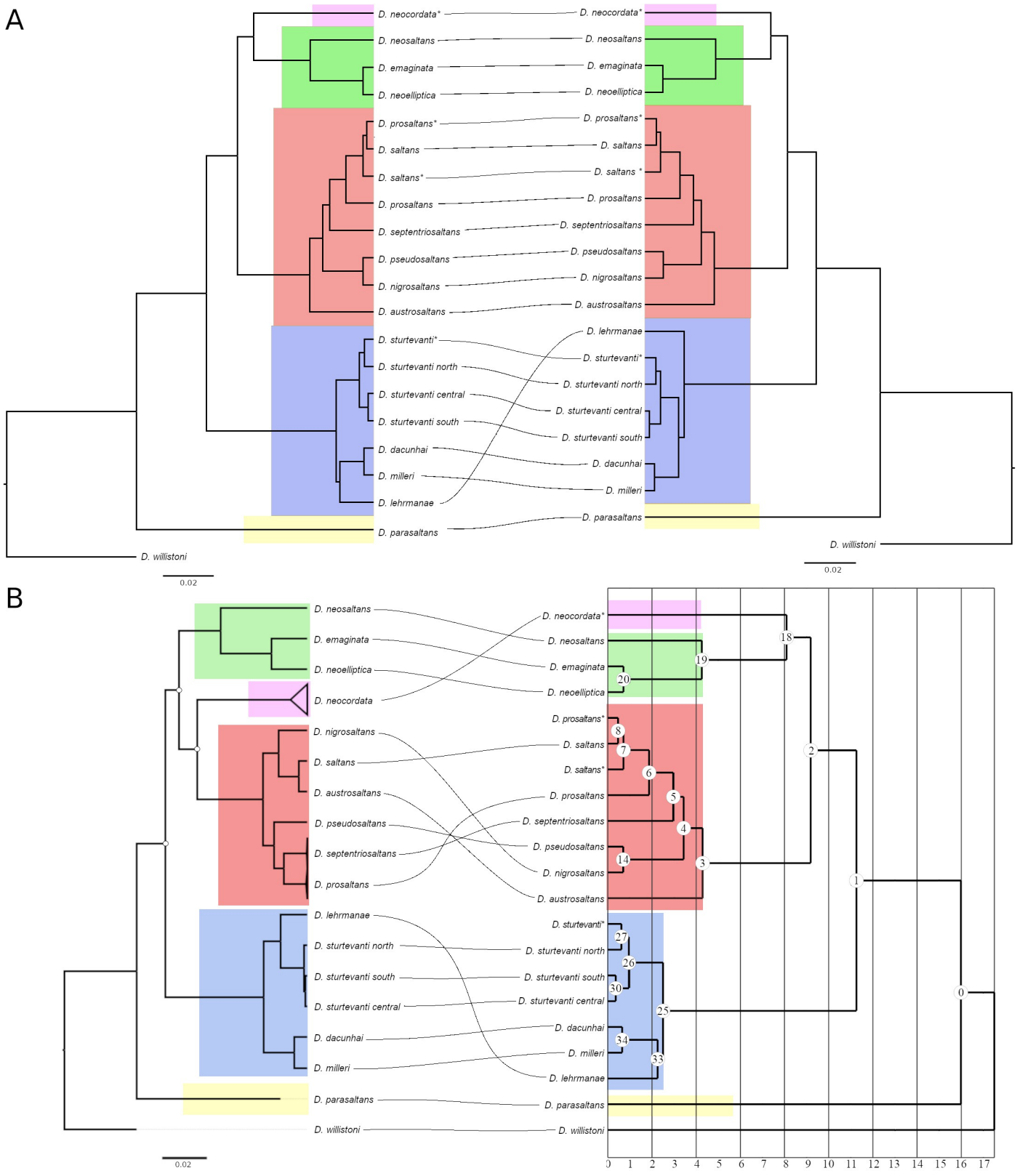
A
D. neocordata*
D. neosaltans
D. emaginata
D. neoelliptica
D. prosaltans*
D. saltans
D. saltans*
D. prosaltans
D. septentriosaltans
D. pseudosaltans
D. nigrosaltans
D. austrosaltans
D. sturtevanti*
D. sturtevanti north
D. sturtevanti central
D. sturtevanti south
D. dacunhai
D. milleri
D. lehrmanae
D. parasaltans
D. willistoni
0.02
B
D. neosaltans
D. emaginata
D. neoelliptica
D. neocordata
D. nigrosaltans
D. saltans
D. austrosaltans
D. pseudosaltans
D. septentriosaltans
D. prosaltans
D. lehrmanae
D. sturtevanti north
D. sturtevanti south
D. sturtevanti central
D. dacunhai
D. milleri
D. parasaltans
D. willistoni
0.02
0 1 2 3 4 5 6 7 8 9 10 11 12 13 14 15 16 17

Figure 2

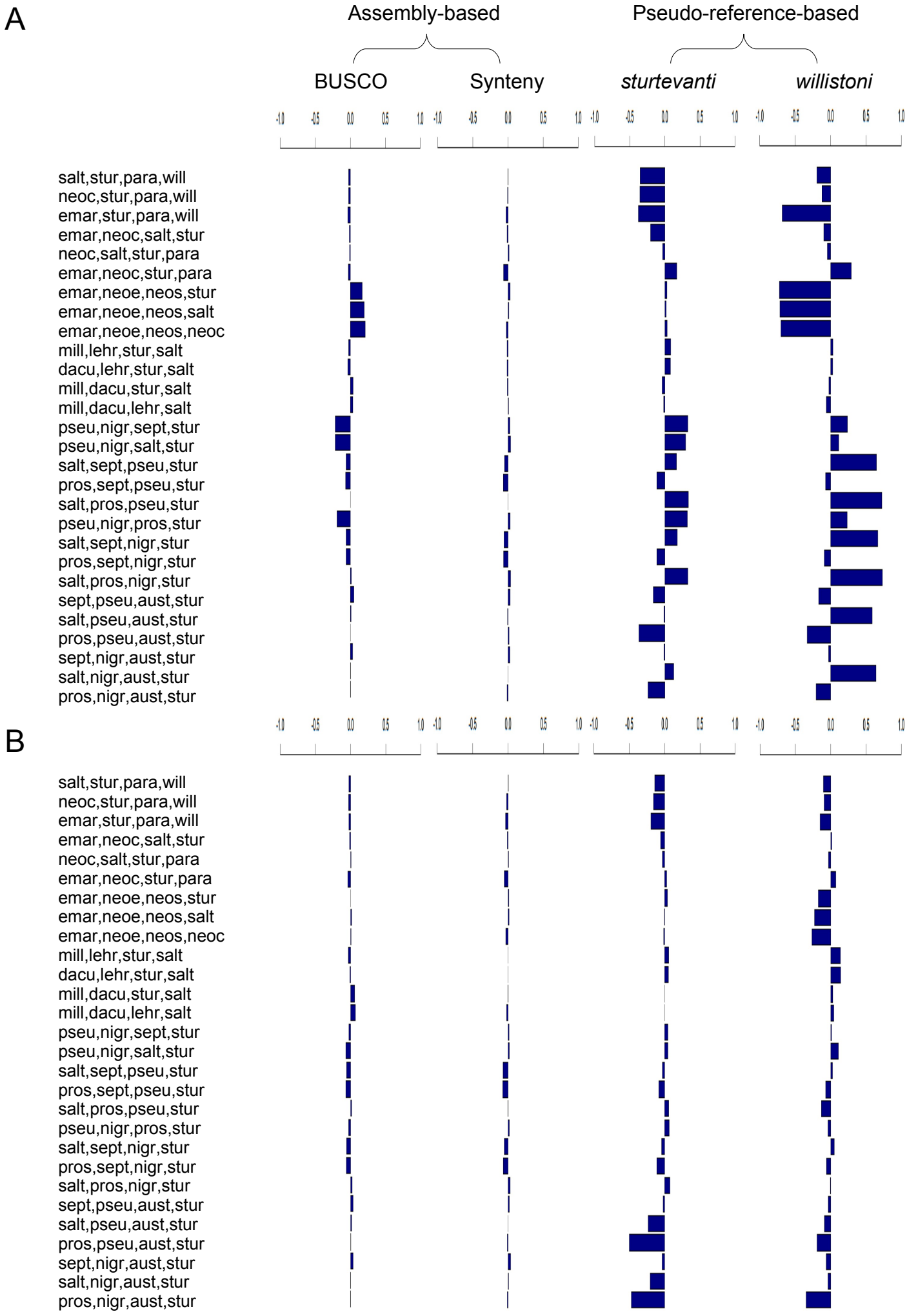
A
Assembly-based
Pseudo-reference-based
BUSCO
Synteny
sturtevanti
willistoni
-1.0
-0.5
0.0
0.5
1.0
salt,stur,para,will
neoc,stur,para,will
emar,stur,para,will
emar,neoc,salt,stur
neoc,salt,stur,para
emar,neoc,stur,para
emar,neoe,neos,stur
emar,neoe,neos,salt
emar,neoe,neos,neoc
mill,lehr,stur,salt
dacu,lehr,stur,salt
mill,dacu,stur,salt
mill,dacu,lehr,salt
pseu,nigr,sept,stur
pseu,nigr,salt,stur
salt,sept,pseu,stur
pros,sept,pseu,stur
salt,pros,pseu,stur
pseu,nigr,pros,stur
salt,sept,nigr,stur
pros,sept,nigr,stur
salt,pros,nigr,stur
sept,pseu,aust,stur
salt,pseu,aust,stur
pros,pseu,aust,stur
sept,nigr,aust,stur
salt,nigr,aust,stur
pros,nigr,aust,stur
B

Figure 3

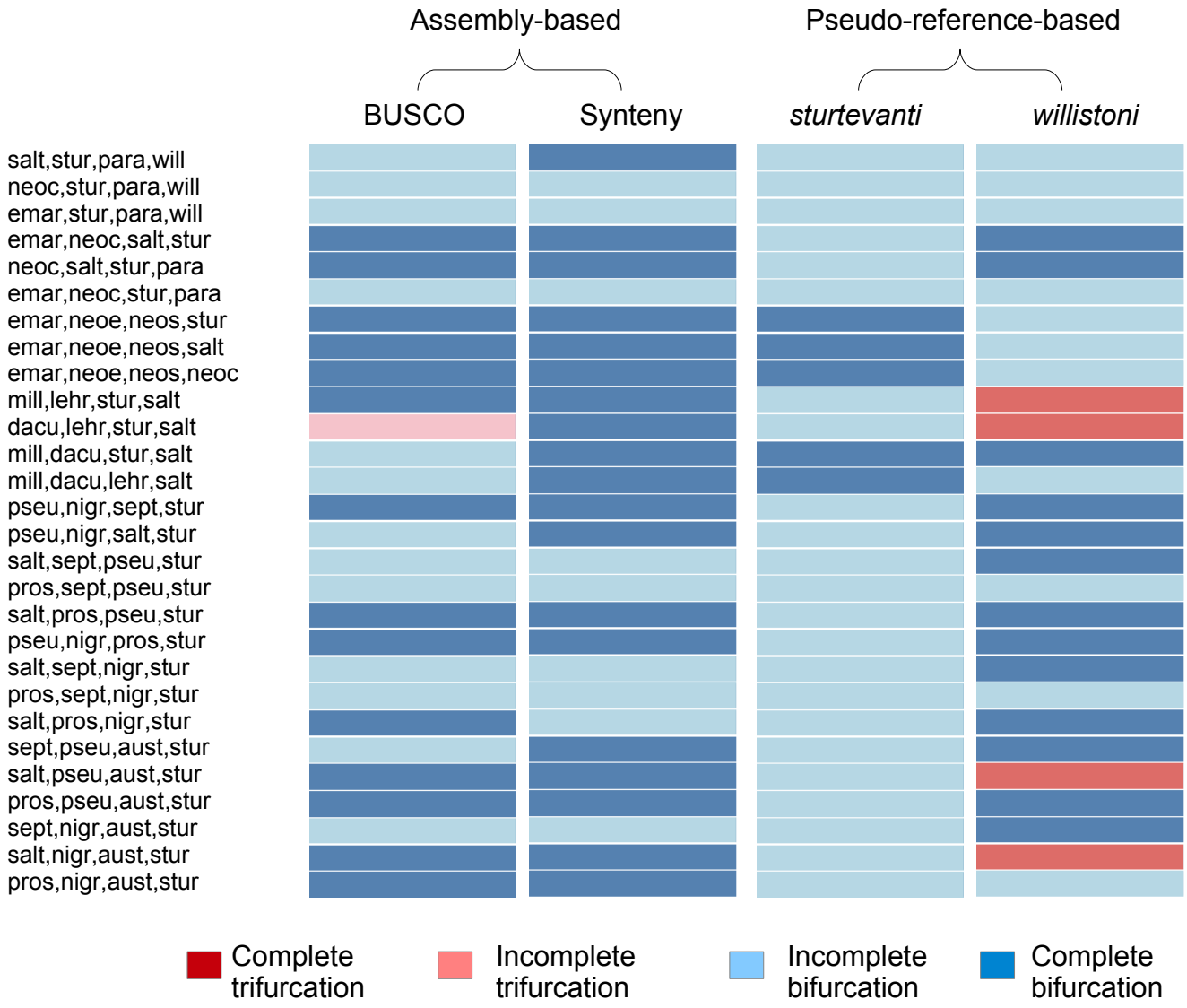
Assembly-based
Pseudo-reference-based
BUSCO
Synteny
sturtevanti
willistoni
salt,stur,para,will
neoc,stur,para,will
emar,stur,para,will
emar,neoc,salt,stur
neoc,salt,stur,para
emar,neoc,stur,para
emar,neoe,neos,stur
emar,neoe,neos,salt
emar,neoe,neos,neoc
mill,lehr,stur,salt
dacu,lehr,stur,salt
mill,dacu,stur,salt
mill,dacu,lehr,salt
pseu,nigr,sept,stur
pseu,nigr,salt,stur
salt,sept,pseu,stur
pros,sept,pseu,stur
salt,pros,pseu,stur
pseu,nigr,pros,stur
salt,sept,nigr,stur
pros,sept,nigr,stur
salt,pros,nigr,stur
sept,pseu,aust,stur
salt,pseu,aust,stur
pros,pseu,aust,stur
sept,nigr,aust,stur
salt,nigr,aust,stur
pros,nigr,aust,stur
Complete trifurcation
Incomplete trifurcation
Incomplete bifurcation
Complete bifurcation

Figure 4

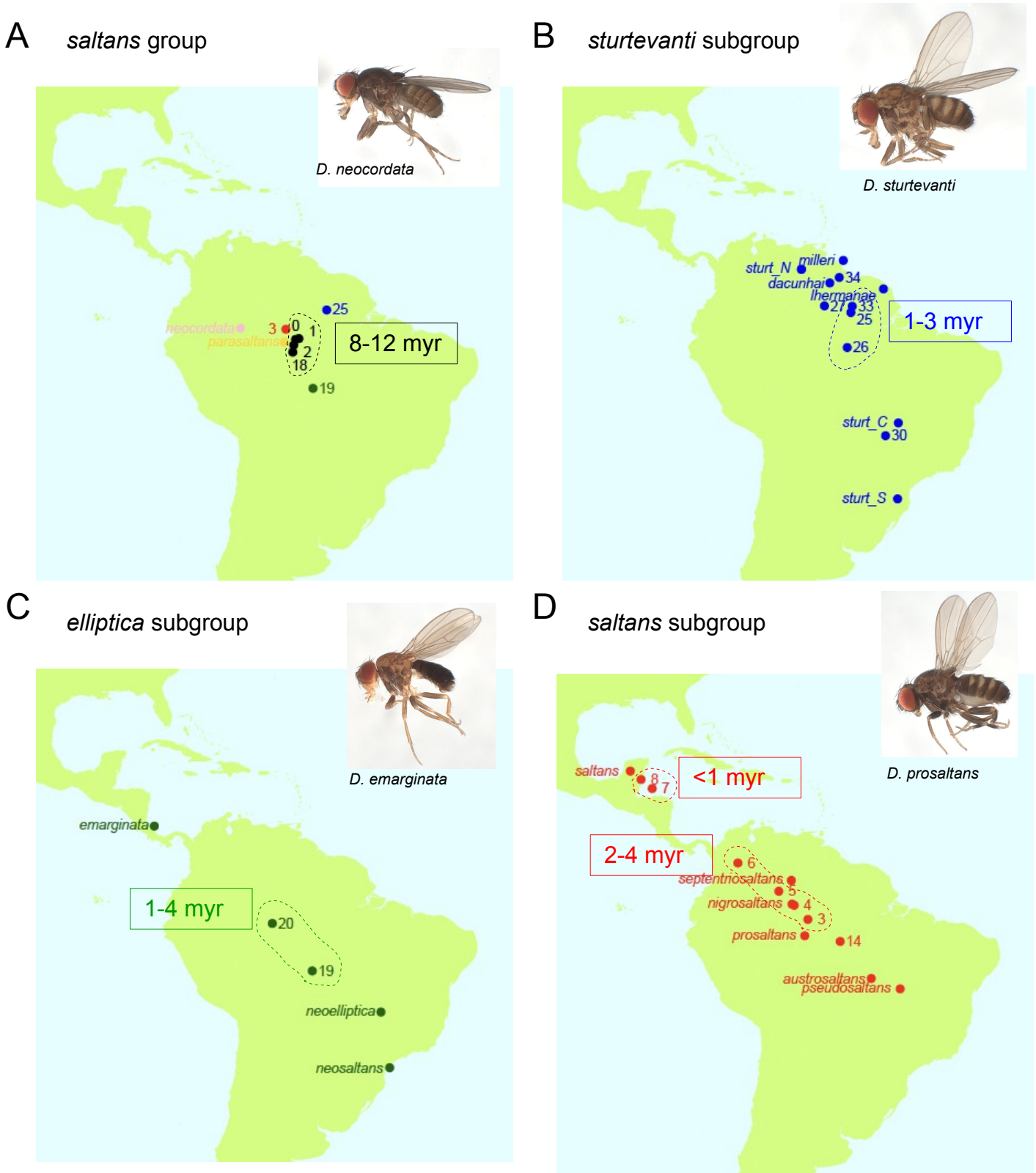
A
saltans group
D. neocordata
neocordata
parasaltans
3
0
1
2
18
25
19
8-12 myr
B
sturtevanti subgroup
D. sturtevanti
sturt_N
milleri
dacunhai
34
lhermanae
27
33
25
26
1-3 myr
sturt_C
30
sturt_S
C
elliptica subgroup
D. emarginata
emarginata
1-4 myr
20
19
neoelliptica
neosaltans
D
saltans subgroup
D. prosaltans
saltans
8
7
<1 myr
2-4 myr
6
septentriosaltans
5
nigrosaltans
4
3
prosaltans
14
austrosaltans
pseudosaltans

Figure 5

List of Supplementary Figures

Figure S1 – Phylogenetic relationships inferred using BEAST from BUSCO genes concatenated according to their Muller's element.

Figure S2 – Phylogenetic relationships inferred using IQ-TREE from BUSCO genes concatenated according to their Muller's element.

Figure S3 – Phylogenetic relationships inferred using ASTRAL-III from BUSCO genes concatenated according to their Muller's element.

Figure S4 –The 2A2B test using four locus-definition strategies (see text) across 28 species quartets as measured for every locus A) before and B) after correction for molecular clock (assembly-based approaches) and mapping quality (pseudo-reference approaches). Colors of bars correspond to the four categories presented in Figure 1, with grey bars corresponding to loci with less than 20 evaluated bi-allelic sites.

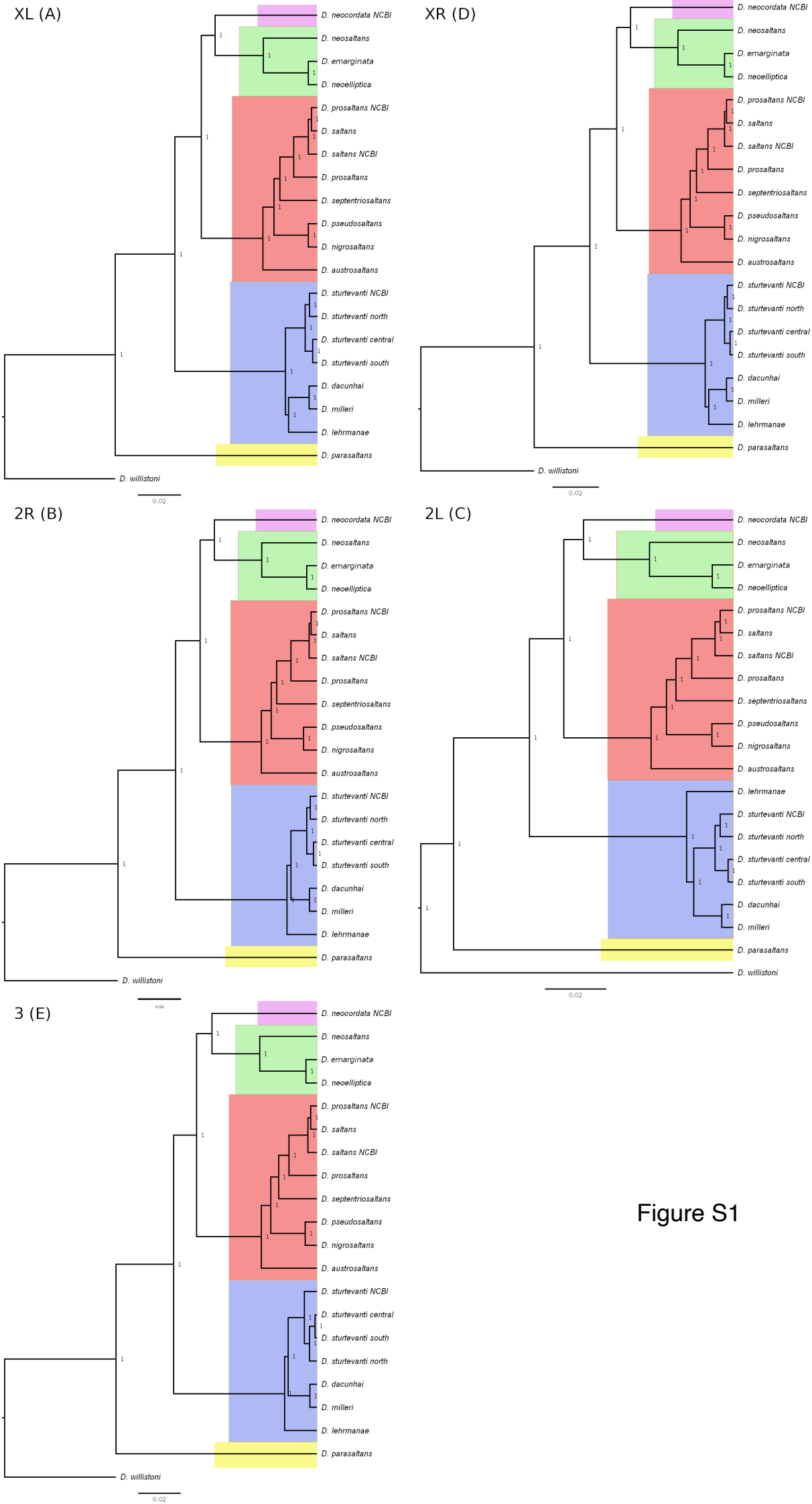
XL (A)
D. neocordata NCBI
D. neosaltans
D. emarginata
D. neoelliptica
D. prosaltans NCBI
D. saltans
D. saltans NCBI
D. prosaltans
D. septentriosaltans
D. pseudosaltans
D. nigrosaltans
D. austrosaltans
D. sturtevanti NCBI
D. sturtevanti north
D. sturtevanti central
D. sturtevanti south
D. dacunhai
D. milleri
D. lehrmanae
D. parasaltans
D. willistoni
0.02
XR (D)
D. neocordata NCBI
D. neosaltans
D. emarginata
D. neoelliptica
D. prosaltans NCBI
D. saltans
D. saltans NCBI
D. prosaltans
D. septentriosaltans
D. pseudosaltans
D. nigrosaltans
D. austrosaltans
D. sturtevanti NCBI
D. sturtevanti north
D. sturtevanti central
D. sturtevanti south
D. dacunhai
D. milleri
D. lehrmanae
D. parasaltans
D. willistoni
0.02
2R (B)
D. neocordata NCBI
D. neosaltans
D. emarginata
D. neoelliptica
D. prosaltans NCBI
D. saltans
D. saltans NCBI
D. prosaltans
D. septentriosaltans
D. pseudosaltans
D. nigrosaltans
D. austrosaltans
D. sturtevanti NCBI
D. sturtevanti north
D. sturtevanti central
D. sturtevanti south
D. dacunhai
D. milleri
D. lehrmanae
D. parasaltans
D. willistoni
2L (C)
D. neocordata NCBI
D. neosaltans
D. emarginata
D. neoelliptica
D. prosaltans NCBI
D. saltans
D. saltans NCBI
D. prosaltans
D. septentriosaltans
D. pseudosaltans
D. nigrosaltans
D. austrosaltans
D. lehrmanae
D. sturtevanti NCBI
D. sturtevanti north
D. sturtevanti central
D. sturtevanti south
D. dacunhai
D. milleri
D. parasaltans
D. willistoni
0.02
3 (E)
D. neocordata NCBI
D. neosaltans
D. emarginata
D. neoelliptica
D. prosaltans NCBI
D. saltans
D. saltans NCBI
D. prosaltans
D. septentriosaltans
D. pseudosaltans
D. nigrosaltans
D. austrosaltans
D. sturtevanti NCBI
D. sturtevanti central
D. sturtevanti south
D. sturtevanti north
D. dacunhai
D. milleri
D. lehrmanae
D. parasaltans
D. willistoni
0.02

Figure S1

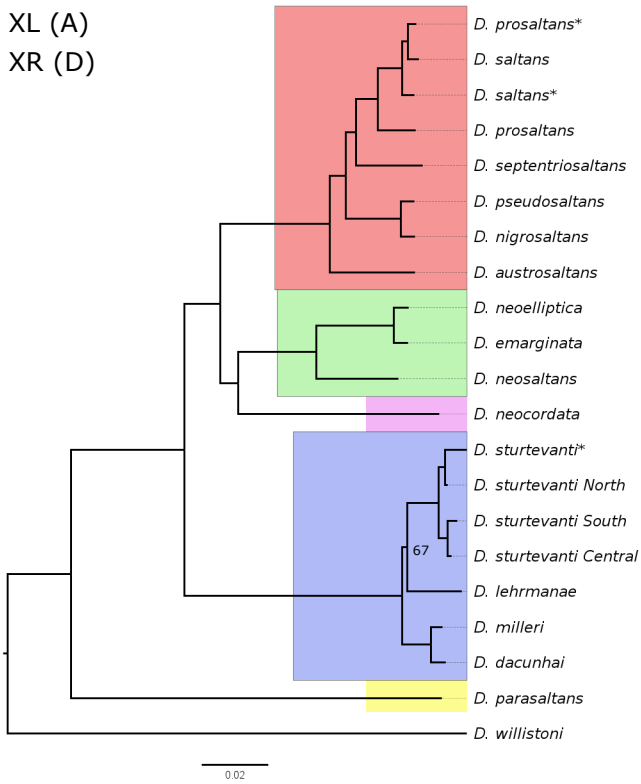
XL (A)
XR (D)
D. prosaltans*
D. saltans
D. saltans*
D. prosaltans
D. septentriosaltans
D. pseudosaltans
D. nigrosaltans
D. austrosaltans
D. neoelliptica
D. emarginata
D. neosaltans
D. neocordata
D. sturtevanti*
D. sturtevanti North
D. sturtevanti South
D. sturtevanti Central
D. lehrmanae
D. milleri
D. dacunhai
D. parasaltans
D. willistoni
67
0.02


D. prosaltans*
D. saltans
D. saltans*
D. prosaltans
D. septentriosaltans
D. pseudosaltans
D. nigrosaltans
D. austrosaltans
D. neoelliptica
D. emarginata
D. neosaltans
D. neocordata
D. sturtevanti*
D. sturtevanti North
D. sturtevanti South
D. sturtevanti Central
D. milleri
D. dacunhai
D. lehrmanae
D. parasaltans
D. willistoni
0.02

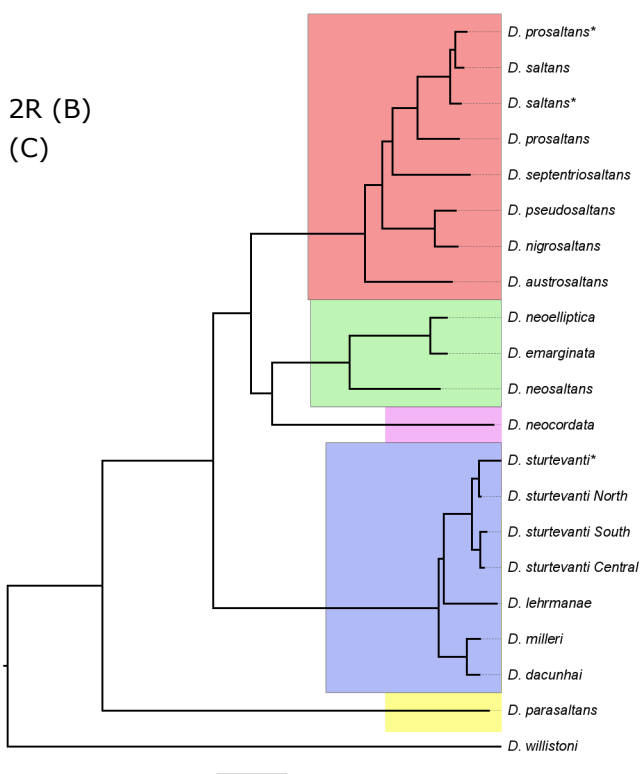
2R (B)
(C)
D. prosaltans*
D. saltans
D. saltans*
D. prosaltans
D. septentriosaltans
D. pseudosaltans
D. nigrosaltans
D. austrosaltans
D. neoelliptica
D. emarginata
D. neosaltans
D. neocordata
D. sturtevanti*
D. sturtevanti North
D. sturtevanti South
D. sturtevanti Central
D. lehrmanae
D. milleri
D. dacunhai
D. parasaltans
D. willistoni
0.02

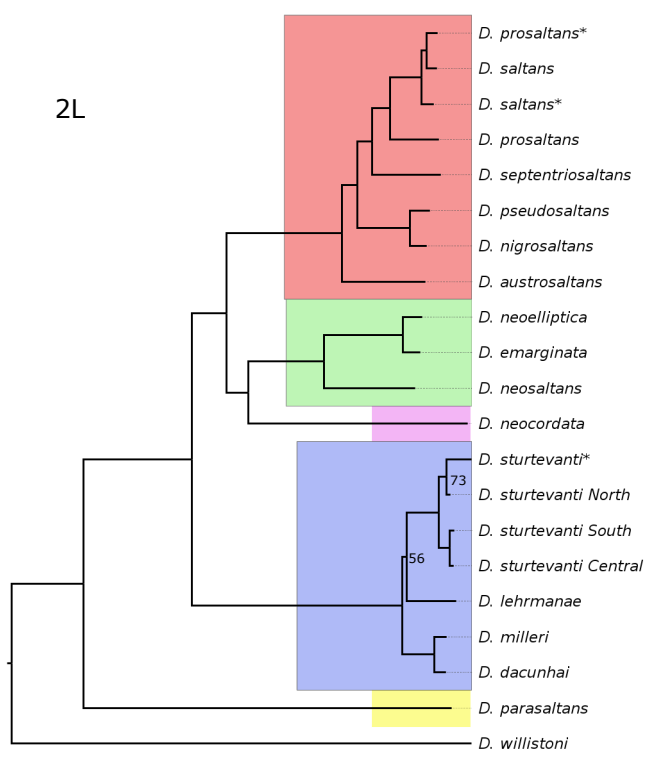
2L
D. prosaltans*
D. saltans
D. saltans*
D. prosaltans
D. septentriosaltans
D. pseudosaltans
D. nigrosaltans
D. austrosaltans
D. neoelliptica
D. emarginata
D. neosaltans
D. neocordata
D. sturtevanti*
D. sturtevanti North
D. sturtevanti South
D. sturtevanti Central
D. lehrmanae
D. milleri
D. dacunhai
D. parasaltans
D. willistoni
73
56
0.02

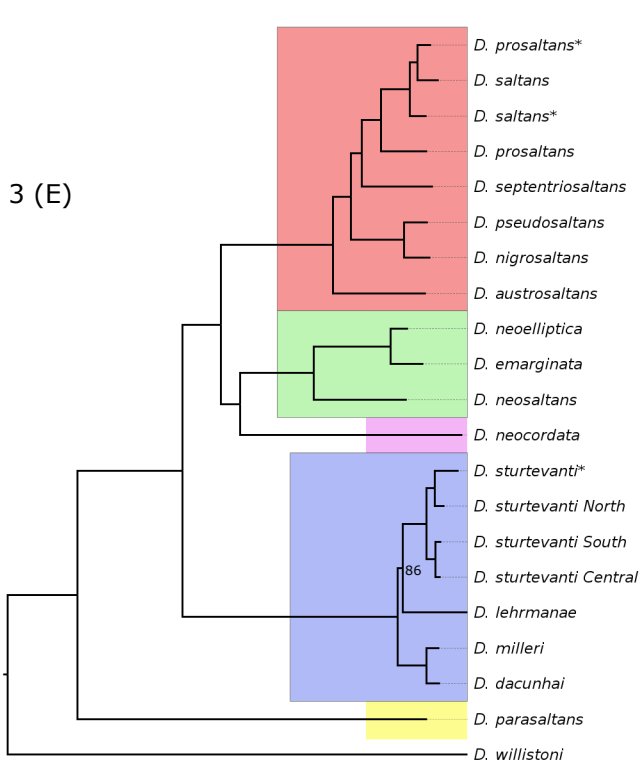
3 (E)
D. prosaltans*
D. saltans
D. saltans*
D. prosaltans
D. septentriosaltans
D. pseudosaltans
D. nigrosaltans
D. austrosaltans
D. neoelliptica
D. emarginata
D. neosaltans
D. neocordata
D. sturtevanti*
D. sturtevanti North
D. sturtevanti South
D. sturtevanti Central
D. lehrmanae
D. milleri
D. dacunhai
D. parasaltans
D. willistoni
86
0.02

Figure S2

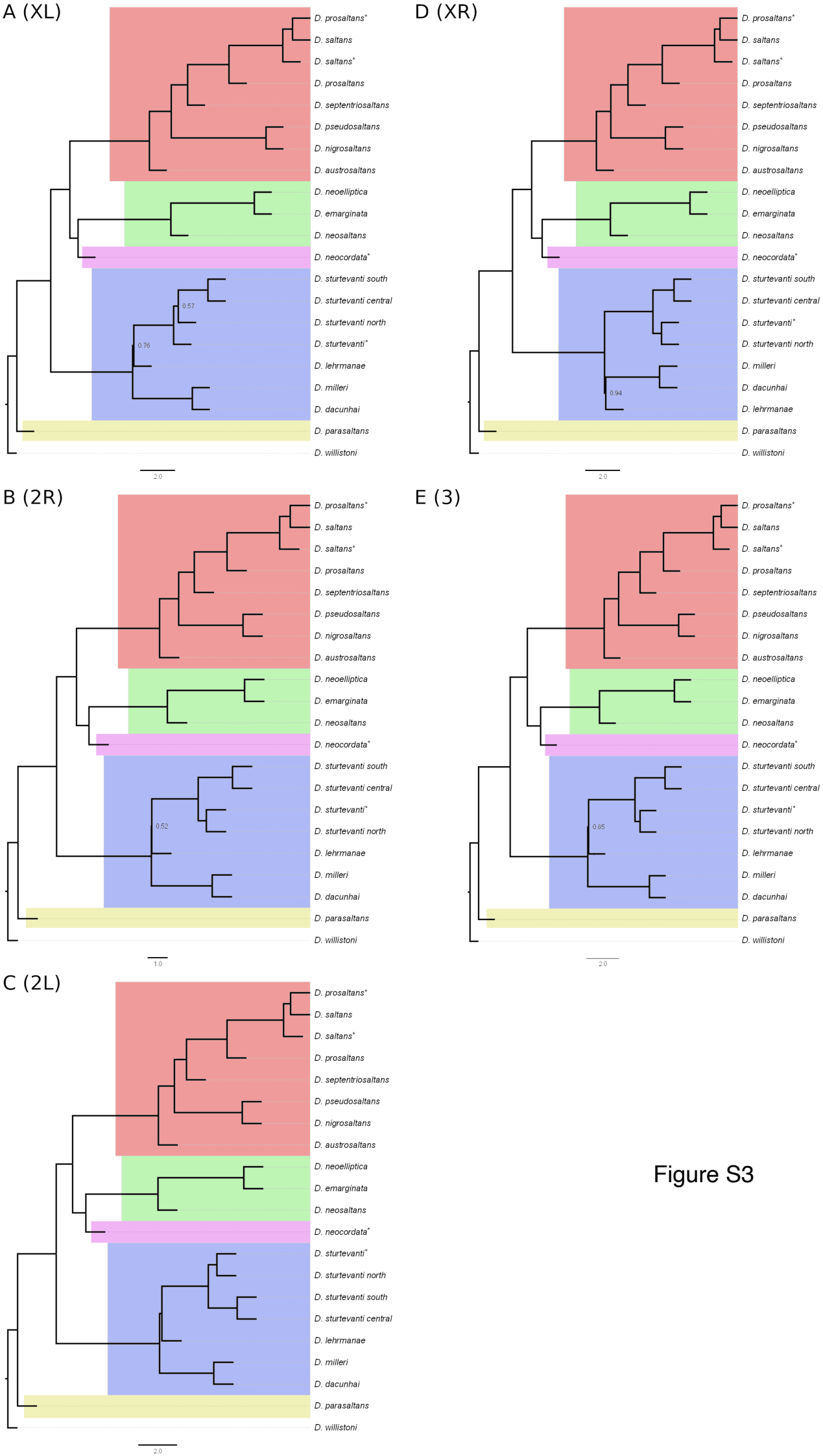
A (XL)
D. prosaltans*
D. saltans
D. saltans*
D. prosaltans
D. septentriosaltans
D. pseudosaltans
D. nigrosaltans
D. austrosaltans
D. neoelliptica
D. emarginata
D. neosaltans
D. neocordata*
D. sturtevanti south
D. sturtevanti central
D. sturtevanti north
D. sturtevanti*
D. lehrmanae
D. milleri
D. dacunhai
D. parasaltans
D. willistoni
0.57
0.76
2.0
D (XR)
D. prosaltans*
D. saltans
D. saltans*
D. prosaltans
D. septentriosaltans
D. pseudosaltans
D. nigrosaltans
D. austrosaltans
D. neoelliptica
D. emarginata
D. neosaltans
D. neocordata*
D. sturtevanti south
D. sturtevanti central
D. sturtevanti*
D. sturtevanti north
D. milleri
D. dacunhai
D. lehrmanae
D. parasaltans
D. willistoni
0.94
2.0
B (2R)
D. prosaltans*
D. saltans
D. saltans*
D. prosaltans
D. septentriosaltans
D. pseudosaltans
D. nigrosaltans
D. austrosaltans
D. neoelliptica
D. emarginata
D. neosaltans
D. neocordata*
D. sturtevanti south
D. sturtevanti central
D. sturtevanti*
D. sturtevanti north
D. lehrmanae
D. milleri
D. dacunhai
D. parasaltans
D. willistoni
0.52
1.0
E (3)
D. prosaltans*
D. saltans
D. saltans*
D. prosaltans
D. septentriosaltans
D. pseudosaltans
D. nigrosaltans
D. austrosaltans
D. neoelliptica
D. emarginata
D. neosaltans
D. neocordata*
D. sturtevanti south
D. sturtevanti central
D. sturtevanti*
D. sturtevanti north
D. lehrmanae
D. milleri
D. dacunhai
D. parasaltans
D. willistoni
0.85
2.0
C (2L)
D. prosaltans*
D. saltans
D. saltans*
D. prosaltans
D. septentriosaltans
D. pseudosaltans
D. nigrosaltans
D. austrosaltans
D. neoelliptica
D. emarginata
D. neosaltans
D. neocordata*
D. sturtevanti*
D. sturtevanti north
D. sturtevanti south
D. sturtevanti central
D. lehrmanae
D. milleri
D. dacunhai
D. parasaltans
D. willistoni
2.0

Figure S3


Assembly-based
Pseudo-reference-based
BUSCO
Synteny
sturtevanti
willistoni
A
salt,stur,para,will
neoc,stur,para,will
emar,stur,para,will
emar,neoc,salt,stur
neoc,salt,stur,para
emar,neoc,stur,para
emar,neoe,neos,stur
emar,neoe,neos,salt
emar,neoe,neos,neoc
mill,lehr,stur,salt
dacu,lehr,stur,salt
mill,dacu,stur,salt
mill,dacu,lehr,salt
pseu,nigr,sept,stur
pseu,nigr,salt,stur
salt,sept,pseu,stur
pros,sept,pseu,stur
salt,pros,pseu,stur
pseu,nigr,pros,stur
salt,sept,nigr,stur
pros,sept,nigr,stur
salt,pros,nigr,stur
sept,pseu,aust,stur
salt,pseu,aust,stur
pros,pseu,aust,stur
sept,nigr,aust,stur
salt,nigr,aust,stur
pros,nigr,aust,stur
B
salt,stur,para,will
neoc,stur,para,will
emar,stur,para,will
emar,neoc,salt,stur
neoc,salt,stur,para
emar,neoc,stur,para
emar,neoe,neos,stur
emar,neoe,neos,salt
emar,neoe,neos,neoc
mill,lehr,stur,salt
dacu,lehr,stur,salt
mill,dacu,stur,salt
mill,dacu,lehr,salt
pseu,nigr,sept,stur
pseu,nigr,salt,stur
salt,sept,pseu,stur
pros,sept,pseu,stur
salt,pros,pseu,stur
pseu,nigr,pros,stur
salt,sept,nigr,stur
pros,sept,nigr,stur
salt,pros,nigr,stur
sept,pseu,aust,stur
salt,pseu,aust,stur
pros,pseu,aust,stur
sept,nigr,aust,stur
salt,nigr,aust,stur
pros,nigr,aust,stur
Unevaluated loci
Complete trifurcation
Incomplete trifurcation
Incomplete bifurcation
Complete bifurcation

Figure S4

List of Supplementary Tables

Table S1 – A synopsis of phylogenetic relationships previously published in the *Drosophila saltans* species group. Species subgroups are represented by the first two letters in capital, whereas species names are represented by the first three letters in small.

Table S2 – Source and genome assembly statistics including BUSCO scores for the genomes used in this study.